Seeing Picasso: an investigation into the visual system of the triggerfish, *Rhinecanthus aculeatus*

Karen L. Cheney[1*], Jemma Hudson[1], Fanny de Busserolles[2], Martin Luehrmann[2], Abigail Shaughnessy[1,2], Cedric van den Berg[1], Naomi F. Green[1], N. Justin Marshall[2], Fabio Cortesi[2*]

[1]School of Biological Sciences, The University of Queensland, Brisbane, QLD 4072 Australia

[2]Queensland Brain Institute, The University of Queensland, Brisbane, QLD 4072 Australia

*corresponding authors: k.cheney@uq.edu.au and f.cortesi@uq.edu.au

Keywords (3-6 words): behaviour, colour vision, opsin, gene expression, visual pigment, retinal topography, visual acuity

Summary statement: Triggerfish, *Rhinecanthus aculeatus*, are ideal species for behavioural investigations of visual processes. Here we show they express six opsin proteins in different photoreceptors, and their visual acuity is significantly better for achromatic stimuli than for chromatic stimuli.

Abstract

Vision is used by animals to find food and mates, avoid predators, defend resources, and navigate through complex habitats. Behavioural experiments are essential for understanding animals' perception but are often challenging and time-consuming; therefore, using species that can be trained easily for complex tasks is advantageous. Picasso triggerfish, *Rhinecanthus aculeatus*, have been used in many behavioural studies investigating vision and navigation. However, little is known about the molecular and anatomical basis of their visual system. We addressed this knowledge gap here and behaviourally tested achromatic and chromatic acuity. In terms of visual opsins, *R. aculeatus* possessed one rod opsin gene (*RH1)* and at least nine cone opsins: one violet-sensitive

SWS2B gene, seven duplicates of the blue-green-sensitive *RH2* gene *(RH2A, RH2B, RH2C1-5),* and one red-sensitive *LWS* gene. However, only five cone opsins were expressed: *SWS2B* expression was consistent, while *RH2A, RH2C-1* and *RH2C-2* expression varied depending on whether fish were sampled from the field or aquaria. Levels of *LWS* expression were very low. Using fluorescent in situ hybridisation, we found *SWS2B* was expressed exclusively in single cones, whereas *RH2A* and *RH2Cs* were expressed in opposite double cone members. Anatomical resolution estimated from ganglion cell densities was 6.8 cycles per degree (cpd), which was significantly higher than values obtained from behavioural testing for black and white achromatic stimuli (3.9 cpd) and chromatic stimuli (1.7-1.8 cpd). These measures were twice as high as previously reported. This detailed information on their visual system will help inform future studies with this emerging focal species.

Introduction

Behavioural evidence of colour vision in non-human animals was first demonstrated in bees over 100 years ago (von Frisch, 1914). Since then, behavioural experiments have been conducted with a range of animal species to investigate the mechanisms that underly colour and other visual processes (reviewed in Kelber et al., 2003). Furthermore, psychophysical experiments have explored higher-order neural processes such as colour constancy (e.g. Olsson et al., 2016), generalization (e.g. Baddeley et al., 2001) and categorization (e.g. Caves et al., 2018; Jones et al., 2001). However, behavioural experiments with animals are often challenging and time-consuming; therefore, it can be advantageous to use species that can be trained easily and perform complex tasks well. Historically, terrestrial animals such as honeybees, birds (e.g., chicks, finches, budgerigars, blue tits), lizards and mice have performed well in such studies (e.g., de Ibarra et al., 2002; Lind and Kelber, 2011; Silvasti et al., 2021; Stoddard et al., 2020). Focal teleost species have included zebrafish, goldfish, sticklebacks, cichlids, guppies, and damselfish (e.g., Escobar-Camacho et al., 2019; Neumeyer, 1985; Neumeyer, 1986; Neumeyer, 1992; Risner et al., 2006; Sibeaux et al., 2019; Siebeck et al., 2008).

Over the past decade, a coral reef triggerfish, *Rhinecanthus aculeatus* (Linnaeus, 1758) (commonly known as Picasso or Lagoon triggerfish), has been used in a number studies on visual processes, including the role of double cones (two single cones joined together) (Pignatelli et al., 2010), colour discrimination thresholds (Champ et al., 2016; Cheney et al., 2019), the perception of visual illusions (Simpson et al., 2016), impact of

caustics on object detection (Matchette et al., 2020), the segregation of objects (Mitchell et al., 2017) and context-dependent luminance perception (van den Berg et al., 2020). *Rhinecanthus aculeatus* has also been used to understand how animals collect, process, and use spatial information to accurately navigate through their environment (Karlsson et al., 2019), for bioinspired fish robots (Hu et al., 2006) and provide an example of unusual sound production in teleosts (Parmentier et al., 2017). They are ideal for behavioural studies as they are relatively easy to keep, have a bold personality and can be trained for complex tasks using operant conditioning. However, a detailed molecular and anatomical investigation of their visual system is needed to help interpret behavioural results, which we present in this study.

In common with other vertebrates, the photoreceptor cells of fish are in a backward-facing layer at the back of the retinas, and contain visual pigments, constructed from an opsin protein with a centrally bound light-sensitive retinal chromophore (reviewed in Musilova et al., 2021). The visual pigment absorbs light and initiates the phototransduction cascade, which converts the light input into electric signals. These signals are carried through several neuronal layers before reaching the ganglion cells that converge into the optic nerve. It is the number and spacing of the ganglion cells that provide the upper limit for spatial resolution or visual acuity. Teleosts often show specialisation in ganglion- and photoreceptor-cell densities and distribution that reflect their specific ecologies. Fishes that live in highly complex 3D visual environments such as coral reefs often have concentric areas of higher cell densities that improve visual resolution along their main visual axes. Contrary, teleosts that occupy simpler visual environments such as at the sand water interface, have horizontal streaks of higher cell densities that assist in scanning the horizon for food or predators (reviewed in Cortesi et al., 2020).

To perceive colour, animals must have at least two photoreceptor types with different spectral sensitivities, and the relative excitation ratios from each photoreceptor type are compared in a colour opponency process. The peak spectral sensitivity (λ_{max}) of the visual pigment depends both on variability in key opsin amino acids in the retinal binding pocket and the chromophore type used: vitamin A1-based pigment is shorter shifted compared to vitamin A2-based chromophore (reviewed in Carleton et al., 2020). Vertebrate visual opsins are classified into five types based on their photoreceptor specificity, phylogeny and the λ_{max} they confer. These five visual opsins were most likely already present in the vertebrate ancestor (Collin et al., 2003) and encode one rod opsin (rhodopsin, RH1, teleost λ_{max} = 447-

525 nm) and four cone opsins: a short-wavelength-sensitive protein class 1 opsin (SWS1) maximally sensitive to UV–violet wavelengths (347–383 nm λ_{max}), a second short-wavelength-sensitive class opsin (SWS2) maximally sensitive to the violet–blue part of the spectrum (397–482 nm λ_{max}), a middle-wavelength-sensitive class 2 rhodopsin-like opsin (RH2) maximally sensitive to blue–green wavelengths (452–537 nm λ_{max}) and a long-wavelength-sensitive class opsin (LWS) maximally sensitive to the green–red part of the light spectrum (501–573 nm λ_{max}) (Carleton et al., 2020). SWS proteins are usually found in single cones, whereas RH2 and LWS opsins occur in double cones (Carleton et al., 2020).

Previously, the spectral sensitivities of *R. aculeatus* photoreceptors were measured using microspectrophotometry (MSP) (Cheney et al., 2013). *R. aculeatus* has a single cone which houses a short-wavelength pigment (413 nm λ_{max}), while medium (480 nm λ_{max}) and long-wavelength pigments (528 nm λ_{max}) are housed separately in the two members of the double cone. *R. aculeatus* also use the two members of the double cone independently in colour vision, facilitating trichromatic colour perception (Pignatelli et al., 2010). This suggests that - unlike birds, for example - some fish may not have photoreceptors specialised for either chromatic or achromatic vision (but see the review by Baden, 2021) on visual circuits in zebrafish). However, little is known about the molecular basis of vision in this species. We therefore first used whole genome sequencing and high-throughput RNA sequencing (RNAseq) to determine opsin gene repertoire and opsin expression. Second, with each expressed opsin sequence and known data on spectral tuning sites, the spectral sensitivity for each opsin class was predicted to examine whether it compared with previously published MSP data (Cheney et al., 2013). We then used fluorescent in situ hybridisation (FISH) to determine opsin specificity to single and double cone types.

Finally, we used an integrative approach to examine visual acuity in this species using retinal topography of photoreceptor and ganglion cells across the retina, and behavioural acuity experiments of both achromatic and isoluminant chromatic gratings using a paired-choice test with square wave gratings. Previous behavioural testing with this species using achromatic black and white gratings suggests that this species has a visual acuity of 1.75 cycles per degree (cpd) (Champ et al., 2014). However, anatomical investigations of triggerfish suggest higher possible visual acuity of 3.4 cpd for ganglion cells (Champ et al., 2014). Spatial contrast sensitivity may be higher for achromatic gratings than for chromatic gratings, which has been shown in other vertebrates, including humans and birds (Lind and Kelber, 2011; Mullen, 1985). In this study, we provide a deeper investigation into the visual

system of this emerging focal species, which we hope will inform future studies of visual perception and navigation.

Material and methods

Study species and specimen collection

Rhinecanthus aculeatus are common reef fish found on shallow sub-tidal reef flats across the Indo-Pacific region and are generalist omnivores known to feed on a varied diet including algae, detritus, molluscs, and crustaceans (Randall et al., 1997). Individuals (n = 23) were caught using clove oil and hand nets from shallow reefs surrounding Lizard Island, Great Barrier Reef, Australia, or obtained from an aquarium supplier (Cairns Marine Pty Ltd; Cairns, Australia) between 2017 and 2020. Fish ranged in size from 8.1 to 20.6 cm (standard length, SL) and were collected under a Queensland General Fisheries Permit (183990) and Great Barrier Reef Marine Park Authority Permit (G16/38497.1). Sex and age were not determined. Experiments were approved by the University of Queensland Animal Ethics Committee (2017/AEC000077 and QBI/304/16).

For molecular and anatomical techniques, fish (n = 15) were anaesthetized with clove oil (10% clove oil; 40% ethanol; 50% seawater) and then euthanised. Eyes were enucleated, then the cornea and lens were removed. This species has a yellow corneal pigment (Siebeck and Marshall, 2001), the density of which increases across the cornea during the day (N. F. Green, unpublished observations). Depending on the analysis, the eyes were preserved in different fixative solutions. Eyes that were allocated to retinal mapping were fixed overnight in 4% paraformaldehyde (PFA) and stored at 4°C. Following this, these eyes were stored in 0.1 M phosphate-buffered saline (PBS; pH 7.4) until further analysis. For RNA sequencing, eretinas were dissected out of the eyecup and preserved in RNAlater (Ambion) at −20°C until extraction. For FISH, retinas were prepared following the protocol in Barthel and Raymond (2000) and fixed in 4% PFA at 4°C overnight, washed twice for 5 min in PBS and rinsed briefly in 70% MetOH, before being transferred to 100% methanol and stored at -20°C until use. One individual was fin clipped and the tissue was preserved on 100% ethanol for genome sequencing.

For behavioural experiments, fish (n = 8) were transported to the University of Queensland and housed in individual tanks (89 x 41 x 22 cm). Each tank had continuously flowing water supplied by a sump system and air stones to oxygenate the water.

Transcriptome and genome sequencing, quality filtering and de novo assembly

The retinal transcriptomes of five *R. aculeatus* were sequenced according to (Musilova et al., 2019). One individual was euthanised immediately after capture from the reefs off Lizard Island, Great Barrier Reef, and four individuals were euthanised after being in aquaria at the University of Queensland for between 10 and 18 months. In summary, total RNA was extracted using a RNeasy midi Kit (Qiagen), and the quality and concentration of the RNA was checked using a Eukaryotic Total RNA Nanochip on an Agilent 2100 BioAnalyzer. The transcriptome sequencing and RNAseq libraries (paired end, 150bp insert) was outsourced to Novogene (novogene.com). The transcriptome filtering and de novo assembly was performed following the protocol described in (de Busserolles et al., 2017). Briefly, the raw reads were uploaded to the Genomics Virtual Laboratory (v.4.0.0) (Afgan et al., 2015) on the Bioinformatics platform Galaxy Australia (https://usegalaxy.org.au/). Using FastQC (Galaxy v.0.72) the quality of the sequences was assessed. They were then quality filtered using Trimmomatic (Galaxy v. 0.36.6) (Bolger et al., 2014), followed by the de novo assembly using Trinity (Galaxy v.2.8.5) (Haas et al., 2013). The newly sequenced samples were subsequently combined with three of our previously sequenced wild-caught samples from Lizard Island (Musilova et al., 2019) to make up our *R. aculeatus* opsin expression dataset.

To identify the visual opsin genes from the transcriptomes, further analyses were performed following the detailed protocol in de Busserolles et al. (2017). The assembled transcripts of *R. aculeatus* were mapped to the opsin gene sequences of the Dusky dottyback (*Pseudochromis fuscus*: GenBank accession No.: KP004335.1) using the medium sensitivity (30% max mismatch between transcripts) in Geneious v.2020.1.2 (www.geneious.com). *Pseudochromis fuscus* was chosen because of its relatively close phylogenetic relationship with *R. aculeatus*, as well as having representatives from all five visual opsin gene classes. To ascertain that all opsin genes were correctly assembled, and lowly expressed genes were picked up in the assembly, the filtered, unassembled transcriptome reads were then back-mapped against the extracted opsins' sequences using medium-low sensitivity (20% max mismatch between reads). For *RH2*, we detected extra copies that were only partially assembled or that were misassembled. Hence, in this case we used a read mapping approach to disentangle similar gene copies as per de Busserolles et al. (2017) and Musilova et al. (2019). Filtered, unassembled reads were mapped against the *P. fuscus RH2* reference using medium-low sensitivity settings (20% max mismatch between reads). We then extracted

copy-specific reads by moving along the reference from single-nucleotide polymorphism (SNPs) to SNP. Paired-end information allowed us to bridge the gaps between the SNPs. If the coding region was not completely recovered, we re-mapped unassembled reads using the consensus as a template with low sensitivity settings (0-2% max. mismatch between reads). This allowed us to reconstruct the whole coding region of all expressed *RH2* copies.

To make sure that we did not miss any visual opsin genes that were not expressed in our samples, we sequenced a draft genome for *R. aculeatus* (ID Olaf) using Illumina short-read technology. Genomic DNA was extracted from a fin clip using the Qiagen DNeasy Blood & Tissue kit according to the manufacturers protocol (qiagen.com). DNA quality control (Agilent 5400, agilent.com), library preparation, and sequencing (paired end 150 bp, 350 bp insert) was outsourced to Novogene (novogene.com). Visual opsin genes were subsequently extracted from the genomic raw reads (212'097'824 paired end fragments, 31.8 Gb) using the read-mapping approach as outlined above and detailed in (Musilova et al., 2019). The only difference was that for the genome, we used the raw-reads and mapped them against the single exons of the *P. fuscus* opsins to avoid long-repetitive intronic sequences. The extracted opsin genes from the genome were then combined with the ones mined from the transcriptomes to generate a *R. aculeatus* visual opsin gene dataset.

We used BLAST (http://blast.ncbi.nlm.nih.gov/) to confirm the opsin gene identity and by phylogenetic reconstruction. To obtain the opsin gene phylogeny, the opsin gene sequences of *R. aculeatus* were aligned with a reference data set (obtained from GenBank https://www.ncbi.nlm.nih.gov/genbank) using MAFFT v.7.450 (Katoh and Standley, 2013) with the L-INS-I settings. On the CIPRES platform, jModeltest v.2.1.6 was used to select the most appropriate model of sequence evolution. Following this, MrBayes v.3.2.7a (Ronquist et al., 2012) was used to infer the phylogenetic relationship between the genes. The following parameters were applied: GTR+I+γ model, with two independent MCMC searches (four chains each), 10 million generations per run, a tree sampling frequency of 1,000 generations, and a burn-in of 25%.

Opsin gene expression

For quantitative gene expression, the filtered reads were mapped to the coding regions of the identified opsin genes with high-specificity settings (98% identity, 80bp minimum read overlap) as per the protocol in de Busserolles et al. (2017). The gene-specific proportional expression was calculated as the fraction of all expressed single cone genes for *SWS*s, double

cone genes for *RH2* and *LWS*, and all opsin genes for *RH1* (see Yourick et al., 2019) for a detailed discussion on opsin gene expression calculations).

For each opsin gene (i), the read count (R_i) was normalised to the length of its coding sequence (bp_i):

$$R_{i,normalised} = (R_i / bp_i)$$

The proportion of rod opsin expressed, was calculated as the proportion of RH1($p_{i,rod}$), relative to the total normalised opsin expression (T_{opsin}).

$$p_{i,rod} = (R_{i,normalised} / T_{opsin})$$

The proportional expression of single cones ($p_{i,SC}$), and double cones ($p_{i,DC}$), was calculated by the proportion of the normalised opsin expression ($R_{i,normalised}$), out of the total normalised expression for single (T_{SC}) or double cones (T_{DC}). Depending on what type of cone opsin that gene was expressed in, the two following formulas were used:

$$p_{i,SC} = (R_{i,normalised} / T_{SC})$$
$$p_{i,DC} = (R_{i,normalised} / T_{DC})$$

Fluorescent in-situ hybridisation (FISH)

Dual-labelling FISH was performed on wholemount retinas of one adult, wild-caught *R. aculeatus* following standard protocols (Barthel and Raymond, 2000; Dalton et al., 2015). Previously extracted retinal mRNA was reverse transcribed using a High-Capacity RNA-to-cDNA Reverse Transcription Kit (Applied Biosystems). Riboprobe templates were synthesized from cDNA via standard PCR using Q5 High Fidelity DNA polymerase (New England Biolabs) and opsin specific primers (Table S1). Amplicons were isolated via gel-electrophoresis and gel extraction (Qiagen Gel Extraction Kit), followed by enrichment PCR using gel-extracted amplicons as cDNA template. Primers were designed to bind to the coding sequence of target opsins (*RH2A*, *RH2C*, *SWS2B*), and to contain T3 or T7 RNA polymerase promoter sequences at their 5'-ends (T3, reverse primer; T7, forward primer) to allow subsequent strand-specific RNA transcription from cDNA templates for riboprobe

synthesis. Anti-sense riboprobes were synthesized and labelled with digoxigenin-UTP (DIG) or fluorescein-UTP (FL) using DIG/FL RNA labelling mix (Roche). A single *RH2C* riboprobe, targeting both expressed *RH2C-1* and *RH2C-2* paralogs, was synthesized due to high sequence similarity between these. Hybridised, labelled riboprobes were detected using anti-digoxigenin (Roche) or anti-fluorescein/Oregon Green (ThermoFisher) antibodies conjugated to horseradish peroxidase. Fluorescent tagging was performed using Alexa Fluor 594 or 488 dyes with tyramide signal amplification (Invitrogen). Finally, retinas were mounted in 70% glycerol in PBS, photoreceptor side up, on microscopy slides with a coverslip.

Dual (*RH2A/RH2C*) or single (*SWS2B*) labelled photoreceptor cells were visualized and imaged using a CFI Apo Lambda S LWD 40X/1.15 NA water immersion objective on a spinning disk confocal microscope (Diskovery, Andor Technologies, UK) built around a Nikon Ti-E body (Nikon Corporation, Japan) equipped with two Zyla 4.2 sCMOS cameras (Andor Technology), and controlled by Nikon NIS Elements software (Nikon Corporation, Japan). Images were exported in TIF file format and further processed (merging of colour channels, adjusting of brightness, z-stack projection) with ImageJ v.1.52p (National Institute of Health, USA).

Prediction of visual pigment maximal absorbance

Maximal absorbances (λ_{max}) of expressed *R. aculeatus* visual pigments were predicted by comparing opsin amino acid sequences to those of percomorph fish species for which the peak spectral sensitivities of their (A1 chromophore–based) visual pigments were known from *in-vitro* pigment reconstitution (*Oryzias latipes*, RH1: 502 nm λ_{max}, AB180742.1, Matsumoto et al., 2006; *Oreochromis niloticus*, SWS2B: 425 nm λ_{max}, JF262088.1, RH2B: 472 nm λ_{max}, JF262086.1, RH2Aalpha: 528 nm λ_{max}, JF262086.1, LWS: 560 nm λ_{max}, JF262088.1, Spady et al., 2006) and by applying tuning effects to their respective peak spectral sensitivities for substitutions at known tuning sites documented in the literature or substitutions at known tuning sites that match the polarity shift of documented substitutions (e.g., for reviews see Takahashi and Ebrey, 2003; Yokoyama, 2008; Yokoyama and Jia, 2020). For an overview of considered sites and applied effects see Table S3. We used *O. niloticus* RH2Aalpha rather than RH2Abeta as the reference due to its greater amino acid sequence similarity to *R. aculeatus* RH2A. We used *O. niloticus* RH2B as the reference for RH2C1 and RH2C2 due to the lack of *in vitro* characterised RH2Cs (Musilova and Cortesi

2021). Opsin gene sequences were translated into amino acid sequences and aligned using MAFFT (v.7.450) (Katoh and Standley, 2013) in Geneious Prime (v.21.1.1). Bovine rhodopsin (NP_001014890.1) was included in all alignments to identify amino acid residues corresponding to known tuning sites and transmembrane regions according to its crystal structure (Palczewski et al., 2000).

Topographic distribution of ganglion cells and cone photoreceptors

Preparation of retinal wholemounts

Retinal wholemounts were prepared according to standard protocols (Coimbra et al., 2006; Stone et al., 1981; Ullmann et al., 2012). The orientation of the retina was kept by noting the position of the falciform inside the eyecup once the cornea and lens were removed. In all our *R. aculeatus* specimens, the falciform process ended in the ventral margin of the retina. Each retina was bleached overnight at room temperature in a solution of 3% hydrogen peroxide in 0.1 M PBS. For photoreceptor analysis, retinas were whole mounted (photoreceptor layer up) in 100% glycerol on a microscope slide. For ganglion cell analysis, retinas were whole mounted, ganglion cell layer facing up, on a gelatinised slide, left to dry overnight in formalin vapour to improve fixation and cell differentiation (Coimbra et al., 2006; Coimbra et al., 2012), stained in 0.1% cresyl violet (Coimbra et al., 2006) and cover slipped with Entellan New (Proscitech). Possible shrinkage during staining was considered negligible and if present confined to the retina margin, since the retinal wholemount was attached to the slide during the entire staining process (Coimbra et al., 2006).

Stereological analyses and topographic map construction

Following the protocols described in (de Busserolles et al., 2014a; de Busserolles et al., 2014b), topographic distribution of single cones, double cones, total cones and ganglion cells were assessed using the optical fractionator technique (West, 1991) modified by (Coimbra et al., 2012; Coimbra et al., 2009). Briefly, cone photoreceptors and ganglion cells were randomly and systematically counted using the parameters listed in Table 1 and a 63x oil objective (numerical aperture 1.40) mounted on a compound microscope (Zeiss Imager.Z2) equipped with a motorised stage (MAC 6000 System, Microbrightfield, USA), a digital colour camera (Microbrightfield, USA) and a computer running StereoInvestigator software (Microbrightfield, USA). The counting frame and grid size were chosen carefully to maintain the highest level of sampling and achieve an acceptable Schaeffer coefficient of

error [CE <0.1, (Glaser and Wilson, 1998)]. The grid size was adjusted between individuals to take into consideration the variation in size between specimens and allow sampling of around 200 sites per retina (Table 1). To get a more accurate estimate of the retinal ganglion cell peak density, sub-sampling was performed in the highest cell density area using the same counting frame but with half the grid size from Table 1.

Single cones and double cones were easily distinguished and counted separately and simultaneously using two different markers to generate data for single cones alone, double cones alone, and the two cell types combined (total cones). Ganglion cells were arranged in a single layer within the ganglion cell layer that also comprised displaced amacrine cells and glial cells. Since amacrine cells were not easily distinguished from ganglion cells using cytological criteria alone (Collin and Collin, 1988; Hughes, 1975), especially in high density areas, they were included in the cell counts and only glial cells were excluded. While the inclusion of amacrine cells in the analysis usually does not influence the overall topography (Collin and Pettigrew, 1989), it may contribute to a slight overestimation of the peak density of ganglion cells and ultimately to a slight overestimation of spatial resolving power.

Topographic maps were constructed in R v.2.15.0 (R Foundation for Statistical Computing, 2012) with the results exported from the Stereo Investigator Software according to Garza-Gisholt et al. (2014). The Gaussian kernel smoother from the Spatstat package was used (Baddeley and Turner, 2005) and the sigma value was adjusted to the grid size.

Estimation of spatial resolving power

The upper limit of the spatial resolving power (SRP) in cycles per degree was estimated for each individual using the peak ganglion cell density (PDG in cells/mm) as described by (Collin and Pettigrew, 1989). Briefly, the angle a, subtending 1 mm on the retina can be calculated as follows:

$$a = \arctan(1/f)$$

Where f, the focal length or the distance from the centre of the lens to the retina, is 2.55 (Matthiessen's ratio, (Matthiessen, 1882)) times the radius of the lens. Knowing a, the PDG and the fact that two ganglion cells are needed to distinguish a visual element from its neighbour, the SRP in cycles per degree (cpd) can be calculated as follow:

$$SRP = (PDG/a)/2$$

Behavioural measurements of achromatic and chromatic acuity

Experimental setup

We used eight triggerfish (8.1 to 16.5 cm, SL) to measure achromatic and chromatic acuity using a pairwise discrimination behavioural task with square wave gratings (4 x 4 cm; Figure S2). Fish were allowed to acclimatise to their tanks for 2-3 weeks and fed twice a day with a mixture of blended squid, prawns, fish flakes and peas. Tanks were illuminated with 240V/50Hz LED Batten 20W lights (FL2527; Fuzion Lighting, QLD), which were hung at 50 cm above the end of the tank at which the target stimuli were placed. The side-welling irradiance of each tank was measured with an Ocean Optics USB2000 spectrometer with a 400 µm fibre and a cosine corrector (Figure S2). Measurements were taken in the middle of the water column at 10 cm from the end of the divider pointing towards the stimuli.

Each tank was divided into three sections: a holding area and two passages separated by a 50-cm long white opaque Corflute board, down which fish could swim to reach the target stimuli (Figure S2). During testing, a transparent Perspex board was initially placed across the tank at the end of the Corflute divider, which allowed the fish to swim back and forth in front of both stimuli several times before the transparent Perspex board was lifted and they could swim down one passage, which was considered a choice by the fish. This set the point of decision to 50 cm.

We tested black-white square wave achromatic gratings and two combinations of chromatic square wave gratings: green-yellow to mainly stimulate the medium and long cones, and pink-purple to stimulate the short and long cone. Stimuli were between 0.5 to 5 for black-white achromatic stimuli (n = 10 stimuli) and 0.5 and 3 cpd for chromatic stimuli increasing in increments of 0.5 cpd (n = 6 stimuli). A control (‘solid’) stimulus was made using a square wave grating of 11 cpd, which was deemed unresolvable by the triggerfish from previous data (Champ et al., 2014). Overall, the total number of fish that were tested for each colour combination was: achromatic (n = 4), green-yellow (n = 5), pink-purple (n = 5).

Square wave gratings were printed on Steinbeis TrendWhite paper using a Canon LaserJet Pro 400 printer and laminated with 80-micron gloss laminating sheets. We tried to ensure colours within a chromatic combination were as isoluminant as possible (green-yellow, and pink-purple) based on quantum catches for an average of double cone members, which are thought to process luminance information (Pignatelli and Marshall, 2010; van den Berg et al. 2020). To calculate quantum catches, the spectral reflectance of printed colours

was measured under a black cloth covered box with an Ocean Optics USB2000 spectrophotometer (Ocean Optics, Fl, USA), a PX-2 pulsed xenon light source, a 200 µm diameter, bifurcated cable held at 45 degrees 1 mm above the paper. A Spectralon white standard was used to calibrate the spectrophotometer and a piece of black velvet covering the end of the fibre was used as the dark standard. Quantum catches of photoreceptors were quantified using photoreceptor spectral sensitivity of triggerfish (Cheney et al., 2013), illumination and reflectance spectra of printed colours as per equation (1) in Vorobyev and Osorio (1998). Average quantum catch for the double cone output for the grating colours were: Pink 19.3 and Purple 18.3; Green 27.5 and Yellow 27.3; Black 0.8 and White 72.5.

Training

In the first round of testing, each fish was randomly assigned to one of three treatments: black-white (n = 2), green-yellow (n = 3), or pink-purple (n = 3) stimuli (fish were retrained to another treatment in a second round of testing). Within each of these groups, one fish was assigned the control (11 cpd) stimulus as the rewarded (S+) stimulus and the remaining individuals were assigned the striped (0.5 cpd) stimulus as the rewarded (S+) stimulus. This was done to account for any bias in the type of stimulus (control/striped) being learnt. Fish were trained using operant conditioning to approach and peck at a stimulus to receive a food reward. Initially, a small piece (< 5 mm) of squid mantle was stuck (using the natural adhesive properties of squid) on the rewarded stimulus, while the unrewarded stimulus was left without. Once fish had associated the S+ stimulus with a reward, the squid was removed from the stimulus and fish were then only presented with a reward from above on forceps once they had pecked the S+ stimulus.

Before commencing each trial, an opaque corflute board was placed in front of the transparent Perspex board to ensure the fish could not see the stimuli being placed at the end of each passage. Stimuli were placed in the left or right passage using a random number generator to ensure that fish did not develop a side bias. Once stimuli were in place, the opaque board was lifted, and the fish were given 20 seconds to view the stimulus through the transparent Perspex board. The transparent board was then lifted and the side that the fish swam down was recorded. Fish did not peck the stimulus in all cases but were given a food reward for approaching the correct stimulus. In instances when a fish swam down one passage, but then changed direction and then went down the other passage during a trial, only the original choice was recorded. If fish had not swum down one passage within one

minute of the transparent board being lifted, the fish was deemed unmotivated and trials for that fish were stopped for the rest of that session and continued again in the next session. Once fish successfully chose the S+ stimulus > 80 % of the time over 4 sessions, fish moved on to the testing phase. It took 3-4 weeks to train most fish (total of 20-29 sessions for each); however, one fish only took 1 week (9 sessions) to reach the required standard for testing.

Testing

Testing trials were conducted as per training methods, and 1-2 sessions were conducted each day with a minimum of two hours between sessions. The training stimulus (0.5 cpd) was used as reinforcement through the testing phase and was presented 20-98 times per fish, depending on the individual. Each grating between 1.0 and 3.0 cpd was presented to each fish 7-20 times for black-white achromatic stimuli and 9-30 times for chromatic stimuli. Once fish had completed testing with their first treatment stimuli (black-white, green-yellow, or pink-purple), they were randomly assigned to one of the other two treatments, then trained and tested again as above. However, two fish only completed one treatment due to the time taken for training and testing. In total, 2418 trials were conducted with each grating presented 110 $\pm$ 14 times (mean $\pm$ s.e.) (Table S4).

Data analysis

Data analysis for the behavioural experiment was done in RStudio v.1.3.1056 (Team, 2020). We used the R package quickpsy v.0.1.5.1 (Linares and Lopez-Moliner, 2016) to produce logistic functions for all fish for each target colour set (goodness of fit: deviance < 8.6, P > 0.47). Our response variable was whether the fish chose (1) or did not choose (0) the positive S+ stimulus. We then used the function 'threshold' to interpolate the 62% threshold, which corresponds to a correct choice frequency significantly different from random behaviour, assuming a binomial distribution of the pooled data per grating (n = 110, p < 0.01, one-tailed binomial test). Once thresholds were calculated for each fish, we tested for significant differences between treatments using a General Linear Mixed Model with the lme4 package v. 1.1-27.1 (Bates et al., 2015) and the function lmer. Fish ID was included as a random variable. We produced p-values using the lmerTest package v.3.1-3 (Kuznetsova et al., 2017). There was no difference in whether fish were trained to receive a food reward from the control stimulus (11 cpd) or the grated stimulus ($t_{6.4}$ = 0.15, p = 0.88); fish did not perform differently within a colour treatment between the first and

second sessions ($t_{3.3}$ = 0.60, p = 0.59) and there was no effect of the size of the fish on the visual acuity (z = 0.67, p = 0.51); therefore these factors were excluded from the final analysis.

Results

Opsin gene repertoire

The *R. aculeatus* genome contained one rod opsin gene (*RH1*) and at least nine cone opsins: one violet-sensitive *SWS2B* gene, seven duplicates of the blue-green-sensitive *RH2* gene *(RH2A, RH2B,* and *RH2C1-5),* and one red-sensitive *LWS* gene. For *RH2B* and *RH2C-4* and *RH2C-5*, only the first two exons could be annotated using the whole-genome read-mapping approach. This is because the intron between exons 2 and 3 of *RH2* is too long to be reconstructed using the short reads alone (for details see Musilova and Cortesi, 2021). A high-resolution *R. aculeatus* genome based on long-read technology will be needed in the future to resolve these genes and to assess if even more copies are present. Except for *RH2B* and three *RH2C* copies (*RH2C3-5*), all other opsins were recovered from the transcriptomes. The phylogenetic reconstruction confirmed the class of each opsin gene identified (Figure 1).

Opsin gene expression

The retina of *R. aculeatus* was rod dominated, where *RH1* was expressed on average 68.9% ± 3.75% (n = 8, mean ± s.e.m.). *SWS2B* accounted for 100% of the cone opsin expression in single cones. For the double cone opsins, there was change in expression of the *RH2* and *LWS* genes in relation to whether fish were housed in aquaria or sampled directly from the field. Aquarium fish kept for behavioural trials showed higher *RH2A* expression (n = 4, 60.30 ± 1.65%) compared to individuals sampled directly from the field (n = 4, 35.04 ± 4.38%). However, *RH2C-2* was expressed at higher levels for individuals collected directly from the field (45.89 ± 2.12%) compared to aquarium individuals (27.38 ± 3.81%). *RH2C-1* was expressed similar between field site collected (17.34 ± 4.55%) and aquarium individuals (12.14 ± 2.17%). In addition, *LWS* was expressed at low levels for both aquarium and field site collected individuals (field site: 1.70 ± 1.23 %, aquarium: 0.18 ± 0.09%) (Figure 2).

Fluorescent in-situ hybridisation (FISH)

Double labelling RNA fluorescence in-situ hybridisation of expressed opsin mRNAs in *R. aculeatus* wholemount retinas showed that medium wavelength opsins identified from the retinal transcriptome, *RH2A* and *RH2Cs* (*RH2C* probes did not discriminate between the two identified *RH2C* paralogs) were expressed in opposite members of double cone photoreceptors across the retina (Figure 3, A-D). The sole single cone opsin identified from the retinal transcriptome, *SWS2B,* was expressed exclusively in single cones (Figure 3, E+F).

Prediction of visual pigment maximal absorbance

Amino acid sequence similarity between *R. aculeatus* opsins and the used reference opsins ranged from 85.5% (51 variable amino acids) for RH2C-1 and RH2C-2 to 94.1% (21 variable amino acids) for RH1 (Table S3). Among variable amino acids, 33% (RH1) to 47% (LWS) (data not shown) lay outside transmembrane regions and were thus unlikely to impact spectral tuning. The numbers of variable amino acids across transmembrane regions ranged from 15 in RH1 to 32 in SWS2B, the majority of which were substitutions that did not incur a physicochemical change. One (RH1), five (SWS2B), nine (RH2A), 12 (RH2C-1) and 11 (RH2C-2) were at known tuning sites. However, many of these were undocumented substitutions that did not incur a polarity shift, resulting in consideration of one (RH1), four (SWS2B), three (RH2C-1), two (RH2C-2) and two (RH2A) sites for λ_{max} prediction (Table S3). *R. aculeatus* LWS did not differ from the reference LWS at any known tuning sites.

Predicted *R. aculeatus* visual pigment peak sensitivities only in part matched the cone and rod sensitivities obtained via MSP (Cheney et al. 2013). RH1 was predicted to be maximally sensitive at 500 nm due to S299A (-2 nm; Dungan et al., 2016; Fasick and Robinson, 1998), and closely matched the rod λ_{max} (498 nm) determined using MSP. SWS2B was predicted to be maximally sensitive at 403 nm, primarily tuned to shorter wavelengths compared to *O. niloticus* SWS2B (425 nm) by W265T (-29 nm) and F46V (+8 nm) (Yokoyama et al., 2007). The predicted λ_{max} differed from single cone λ_{max} of 413 nm obtained via MSP. RH2C visual pigments were predicted to be maximally sensitive at 474 nm (RH2C-1) and 476 nm (RH2C-2). Both RH2Cs were slightly red-shifted compared to *O. niloticus* RH2B by primarily M88C (+3 nm; Chinen et al., 2005). RH2C-1 and RH2C-2 differed by only six amino acids (98.3% similarity), with one of these, T266V in RH2C-1, predicted to cause a two nm reduction of its λ_{max} (Chinen et al., 2005). The predicted λ_{max}

are 6 nm (RH2C-1) and 4 nm (RH2C-2) shorter than the peak sensitivity of the shorter medium wavelength sensitive double cone (MWS) determined via MSP (480 nm). RH2A was predicted to be maximally sensitive at 526 nm, with only two sites, C88A (-3 nm; Chinen et al., 2005), and I112V (+1 nm; Chinen et al., 2005), considered to cause a small net blue shift compared to *O. niloticus* RH2Aalpha (528 nm). This predicted λ_{max} almost matched the peak sensitivity of the second, longer MWS double cone in *R. aculeatus* (528 nm) as determined via MSP. Since *R. aculeatus* LWS did not differ from *O. niloticus* LWS at any known tuning sites, its predicted λ_{max} was 560 nm.

We identified several substitutions that, although not previously investigated via site directed mutagenesis (SDM) and *in vitro* pigment regeneration, due to their incurred polarity shifts and the site of their occurrence, may explain the discrepancies between MSP and predicted λ_{max} (see Table S3). In RH1, S166A incurred a polarity shift at a site close to the known RH1 tuning site A164S (Chan et al., 1992) and is also a substitution known to be involved in RH2 tuning (Yokoyama and Jia, 2020). *R. aculeatus* SWS2B showed three polarity changing substitutions, C163F, S166F, and S168A in immediate proximity to the documented tuning site G164A (Yokoyama and Tada, 2003). In both RH2Cs, V185C caused a polarity shift, whereas previously SDM in zebrafish RH2s had shown a -4 nm blue shift for substitution from T to C at this site (Chinen et al., 2005). C98A incurred a polarity shift at a site adjacent to the powerful RH2 tuning site T97A (-8 nm; Takenaka and Yokoyama, 2007). In *R. aculeatus* RH2A, A151T incurred a polarity shift at a site at which SDM from N to S caused a +4 nm red shift in zebrafish RH2 (Chinen et al., 2005).

Retinal topography and anatomical spatial resolving power

The topographic distribution of ganglion cells and cone photoreceptors was analysed in four individuals (two individuals per cell type). Since intraspecific variability in topography pattern was very low for both ganglion cells and cone photoreceptors, only one representative map is presented in Figure 4 and individual maps are provided in the supplementary material (Figure S1).

Ganglion cell topographic distribution revealed the presence of a well-developed horizontal streak with a peak cell density located in the temporal part of the retina (Figure 4) that ranged from 37,161 to 40,125 cells/mm^2 in the two individuals analysed (Table 2). Based on these peak cell densities, estimated spatial resolving power for *R. aculeatus* ranged from 6.4 to 7.2 cycles per degree (Table 2).

Cone photoreceptors in *R. aculeatus* were arranged in a regular retinal mosaic where one single cone was surrounded by four double cones, resulting in a double cone to single cone ratio of 2:1. This mosaic pattern was consistent across the entire retina, resulting in similar topographic distributions for each cone type. As a result, we only present and describe the distribution pattern for the total cone population (Figure 4). Maps for each cone type are provided in the supplementary material (Figure S1). The total cone topography varied slightly from the ganglion cell pattern by having a less developed horizontal streak and a more pronounced area temporalis (Figure 4). However, the peak cell density of total cones which ranged from 64,167 to 70,278 cells/mm^2 (Table 2) was found in the same location (i.e., temporal) as the peak density of ganglion cells. Even though ganglion cells and cone photoreceptor topographies were not analysed in the same retina or individuals, comparison of two individuals of similar size (i.e. ~13 cm SL, individuals 1 and 3), suggested a summation ratio of total cones to ganglion cells in the peak density area of around 2:1.

Behavioural measurements of achromatic and chromatic acuity

Behavioural thresholds (62% correct choice) were significantly higher for black and white achromatic stimuli: cpd = 3.94 (95% confidence intervals, CI: 3.47-4.49) than for green-yellow cpd = 1.71 (CI: 1.46-1.93) ($t_{9.31}$ = -7.39, $p < 0.001$) or for pink-purple cpd = 1.89 (CI: 1.59-2.38) ($t_{7.51}$ = -6.00, $p < 0.001$). Green-yellow and pink-purple treatments were not significantly different from each other ($t_{6.29}$ = 0.58, $p = 0.58$) (Figure 5).

Discussion

Previous microspectrophotometry (MSP) measurements of *R. aculeatus* photoreceptors suggested three spectrally distinct cone types: one blue sensitive single cone (λ_{max} = 413 nm), one blue-green sensitive double cone member (λ_{max}= 480 nm) and a second, green sensitive double cone member (λ_{max}= 528 nm), as well as a single spectral type of rod photoreceptor (λ_{max} = 498 nm) (Cheney et al., 2013). Our transcriptome analysis largely – but not fully – reflects this by revealing the expression of a single rod opsin (*RH1*) and for the cone opsins, a short-wavelength-sensitive opsin (*SWS2B*), yet four medium-long-wavelength-sensitive cone opsins (*RH2C-1*, *RH2C-2*, *RH2A* and *LWS*). Except for one field caught individual, *LWS* expression was at levels barely high enough to reconstruct this gene's coding sequence, suggesting that measured double cone λ_{max} were primarily (if not entirely) due to

the three identified *RH2* opsins. Amino acid-based λ_{max} predictions clarified this picture, indicating that the RH2A visual pigment with a λ_{max} of 526 nm was likely to account fully (i.e., not co-expressed) for the green sensitive double cone member, and this was further supported by our FISH analysis. Predictions also indicated that the two RH2C paralogs were very close in terms of their λ_{max}, and as both showed high expression, either one or both may account for the blue-green sensitive cone member. Unfortunately, due to high mRNA sequence similarity (97.3% identity) our FISH analysis did not allow a distinction between the two expressed *RH2C* paralogs. Co-expression of either of the two *RH2C* paralogs with *RH2A*, in theory, could have explained the discrepancy between predicted RH2C λ_{max} and measured λ_{max} of the blue-green sensitive MWS double cone, a pattern seen for example in some freshwater cichlids (Dalton et al., 2014; Torres-Dowdall et al., 2017). However, our FISH analysis did not show evidence of *RH2A*/*RH2C* co-expression. Instead, it showed these opsins expressed in opposite double cone members, a pattern also observed in other reef fish such as some anemonefishes (Stieb et al., 2019). Taken together, the transcriptome data, visual pigment λ_{max} predictions, and FISH analysis corroborate the existing, MSP-based picture of the Picasso triggerfish photoreceptor spectral sensitivity repertoire.

However, although the number of spectrally distinct photoreceptors might be limited, differences in *RH2* expression between individuals that were sampled in the field and the ones that were kept in aquaria shows that opsin gene expression in adult *R. aculeatus* is plastic over time. As for some freshwater fishes (e.g., cichlids; Nandamuri et al., 2017) and reef fishes (e.g., cardinalfishes and damselfishes; Luehrmann et al., 2018) the change in opsin gene expression in *R. aculeatus* was likely caused by differences in the light environment between the reef and the aquarium. The higher expression of *RH2A* in aquarium held fishes suggests an overall quantitative shift to longer wavelength sensitivity i.e., more long-wavelength-sensitive cones when kept under longer-shifted green/red-dominated LED lights. While it remains to be investigated whether a change in opsin gene expression truly causes a change in visual discrimination, the findings do highlight the importance of assessing an animal's visual system – from molecule to behaviour – in its specific light environment.

Prediction of visual pigment maximal absorbance

We do note that the reliability of predicted visual pigment λ_{max} based on amino acid sequences is inherently limited despite tuning sites and their effects having been extensively studied in many taxa, and in fish arguably more so than in any other vertebrate group (for reviews see Takahashi and Ebrey, 2003; Yokoyama, 2000; Yokoyama and Jia, 2020). Omission of yet unknown tuning sites, effects (if any) of unknown substitutions at known tuning sites, and over- or underestimation of tuning effects due to unknown synergistic effects (including effects that affect visual processing in non-spectral ways, e.g. via modulation of retinal release dynamics; Castiglione and Chang, 2018), are among the shortcomings of this approach (e.g., Chinen et al., 2005; Yokoyama and Jia, 2020). For example, for both RH2Cs the substitution of polar C at site 185, where SDM of polar T to polar C has previously shown to shift λ_{max} by as much as 4 nm (Chinen et al., 2005), could explain some or all of the discrepancy between predictions and MSP. Similarly, the polarity-changing substitutions identified in *R. aculeatus* SWS2B could on their own or by reducing the effect of W265T cause an increase of the pigment's λ_{max}. Consequently, one would consider predictions more robust for more conserved genes (e.g., RH1) or genes in which the extent of λ_{max} variability across many different taxa could be nearly fully described by variations at only a few sites, as is the case for many LWS pigments ('Five-sites rule'; Yokoyama and Radlwimmer, 1998). In contrast, λ_{max} of SWS pigments (SWS1, SWS2As, SWS2B) and RH2 pigments are notoriously difficult to predict due to a plethora of variable sites that have to some extent been implicated with spectral tuning, however complicated by apparent yet not fully understood, synergistic effects (Shi et al., 2001; Yokoyama and Jia, 2020; Yokoyama and Tada, 2003). In future, additional *in vitro* expression and pigment regeneration assays, particularly in non-model organism species, as well as further investigation of possible tuning sites via SDM, could improve the reliability of spectral sensitivity predictions.

Retinal topography and anatomical acuity

In this study, ganglion cell topography showed a complete and well-developed horizontal streak and no additional high-density areas outside the streak. The total cone topography had a less developed horizontal streak and a more pronounced area temporalis. The peak ganglion cell density was found in the temporal retina with an average of 38,643 cells/mm^2, resulting in an acuity estimate of 6.8 cycles per degree. These estimates fit within

the typical range of shallow water reef fishes, which have an anatomical estimate of visual acuity between 4-27 cpd (Collin and Pettigrew, 1989).

The well-defined streak pattern of *R. aculeatus* found in this study is very similar to the pattern found for another triggerfish, *Balistoides conspicillum* (Collin and Pettigrew, 1989). According to the 'terrain theory' (Hughes, 1977), the topography of cells across the retina represents the symmetry of the habitat. Triggerfishes live in open flat areas where they scour the seafloor for potential prey items and have an uninterrupted view of the sand-water horizon; therefore, a horizontal streak may help them scan their environment for potential predators while searching for prey.

For cone densities and distribution, our results were similar to a previous study on *R. aculeatus* (Champ et al., 2014); however, they substantially differed for the ganglion cell analysis, especially in density and acuity estimates. Ganglion cell topography in Champ et al. (2014) revealed the presence of a partial horizontal streak that extends from the nasal to the central retina, as well as several other high-density areas outside the streak. A peak cell density of 12,450 cells/mm^2 was found in the temporal retina, resulting in an acuity estimate of 3.4 cycles per degree. These differences in topography pattern, ganglion cell density and acuity estimate between the two studies could be due to several factors such as differences in individual size, the methods of analysis used and/or issues encountered during sample preparation.

In teleost fishes, ganglion cell densities and topography patterns usually show very little intraspecific variability (e.g. de Busserolles et al., 2014b), except between individuals of different life stages and therefore sizes (Shand, 1997; Stieb et al., 2019; Tettamanti et al., 2019). In terms of cell densities, while larger individuals with larger eyes usually have a higher total number of ganglion cells in their retina, the number of ganglion cells per retinal area is usually smaller (Stieb et al., 2019; Tettamanti et al., 2019). According to this, the lower cell densities found in the previous study compared to ours could have been explained if they had used larger individuals. However, Champ et al. (2014) used similar sized individuals or slightly smaller ones compared to our study (7-12 cm vs 10-17 cm SL), indicating that size is not a likely explanation for the differences in densities observed between the two studies.

In both studies, displaced amacrine cells were included into the ganglion cell counts. Contrary to the present study, Champ et al. (2014) subsequently applied a multiplication factor of 0.76 to all their ganglion cell counts to account for the inclusion of displaced amacrine cells, which could explain some of the discrepancies in densities between the two

studies. However, even if we take this correction into consideration in our study, our peak ganglion cell density is still at least twice what was reported in the previous study. We chose not to apply a correction factor in this study as displaced amacrine cells in coral reef fishes are mainly present in peripheral and non-specialised areas of the retina, and their inclusion in ganglion cell retinal topographic analyses usually have very little impact on the general topography pattern or the peak cell density estimation (Collin and Pettigrew, 1988). Consequently, even though the inclusion of amacrine cells in our study might slightly overestimate the peak density of ganglion cells and therefore acuity, we believe it provides a more accurate estimate than applying a general correction factor.

The most likely explanation for the differences in ganglion cell densities and topography pattern observed between the two studies is sample processing. During the preparation of our retinal wholemounts we found that *R. aculeatus* had very thick vitreous that proves challenging to remove, especially in the centre of the retina along the retinal meridian. During several attempts, which were not included in this study, leftover vitreous resulted in very weak ganglion cell staining making counting unreliable or even unfeasible in certain areas. Similar challenges might have been encountered in Champ et al. (2014) resulting in an under-sampling of the ganglion cell population along the streak. This could explain why an incomplete streak and patchier topography pattern was found in the previous study, as well as why relatively similar ganglion cell densities (i.e. ~ 5,000 cells/mm^2) were found in the dorsal and ventral part of the retina in the two studies, but much lower densities were found along the streak in the previous study.

Behavioural measurements of achromatic and chromatic acuity

For achromatic gratings, we found that *Rhinecanthus aculeatus* had a behavioural acuity of 3.9 cpd, which was significantly lower than anatomical measurements of 6.8 cpd. For fish, anatomical measurements are often higher than those determined using behavioural experiments (e.g. Brokovich et al., 2010; Pankhurst et al., 1993; Parker et al., 2017). Matthiessen's ratio (2.55), which is an average value from a measure range of 2.4-2.82, is used to estimate focal length instead of using the true focal length of the fish and therefore may cause discrepancies in estimations. Second, visual acuity estimates based on ganglion cell counts only represent a theoretical upper limit of visual acuity. This is because not all ganglion cells contribute to visual acuity. For example, in primates, spatial resolving power is set by the midget ganglion cells, which only account for 70-80% of the total ganglion cell

population (Wassle, 2004). Furthermore, the function of different types of retinal ganglion cells varies both temporally and spatially across the retina in zebrafish (Zhou et al., 2020).

Behavioural studies of visual acuity are likely to represent a more accurate estimate of an animal's functional visual abilities than its anatomical visual acuity. Furthermore, experiments that utilise ecologically relevant paradigms to measure acuity should give closer estimates between behavioural and anatomical measured thresholds. For example, Temple et al. (2013) found that the maximum acuity of archerfish was similar to anatomical measurements when fish spat at prey using the area centralis in the ventro-temporal region of the retina. In contrast, optomotor/optokinetic tests provide some measure of average retinal acuity but will not capture the acuity in specialised regions of the retina, such as in the area centralis or fovea. Behavioural measurements of acuity may also vary depending on the stimuli used. Triggerfish did not perform as well in acuity tests when trained to circular stimuli as opposed to grating stimuli of horizontal and vertical stripes (Champ et al., 2013). Furthermore, different acuities were measured when honeybees were presented with radial (sectored) compared to linear (square-wave) gratings (Srinivasan and Lehrer, 1988), which could be explained by orientation specific feature detecting receptive fields (Marr & Hildreth 1980, Marr 2010).

We found that achromatic acuity (3.94 cpd) of triggerfish was significantly higher than chromatic acuity for both the green-yellow (1.71 cpd) or pink-purple (1.89 cpd) stimuli. This supports previous findings in birds, mammals, and bees (Giurfa et al., 1997; Lind and Kelber, 2011; Mullen, 1985); however, in humans and birds, differences in acuity were found between different colour channels. In budgerigars, visual acuity was lower for blue-green than for red-green gratings, which may be explained by lower numbers of SWS cones in the retina compared to MWS and LWS cones (Hart et al., 2000). Similarly in humans, acuity was lower for blue-yellow contrasts than for red-green (Mullen, 1985). However, the black-white achromatic stimulus had higher overall luminance compared to the chromatic stimuli based on double cone quantum catch; this may have also improved acuity for achromatic stimuli.

In conclusion, we hope that data from this study will inform future studies with this species investigating a range of topics including, but not limited to, teleost perception, navigation, and cognition. We believe that Picasso triggerfish will continue to play a key role in contemporary research in these areas due to their versatility as a focal study organism. We highlight the need for further information on the specific chromatic opponent mechanisms in animals, which is currently poorly understood (Baden and Osorio, 2019).

Acknowledgements

We would like to acknowledge the Turrbal, Jagera, Dingaal, Ngurrumungu, and Thanhil people, the Traditional Owners and custodians of the lands on which the University of Queensland and Lizard Island Research station operates. We pay our respects to their ancestors and their descendants, who continue cultural and spiritual connections to Country and recognize their valuable contributions to Australian and global society. We thank the staff at the Lizard Island Research Station for support during field work and Cairns Marine for supplying fish. We would also like to acknowledge Dr. Rumelo Amor from the QBI Advanced Microscopy Facility for technical support and two anonymous reviewers and editor for valuable feedback.

Competing interests

No competing interests declared

Funding

This work was supported by the Australian Research Council [Future Fellowship FT190100313 to K.L.C; Discovery Early Career Researcher Awards: DE180100949 to F.d.B. and DE200100620 to F.C.; and Discovery Projects DP150102710 and DP180102363 to K.L.C, N.J.M and F.C.]. The stereology analyses were performed at the QBI Advanced Microscopy Facility using Stereo Investigator, which was supported by an ARC LIEF grant (LE100100074).

Data availability statement:

All data supporting this manuscript will be made available on UQ eSpace. Genomic and transcriptomic raw-reads and extracted gene sequences will be made available through GenBank (https://www.ncbi.nlm.nih.gov/genbank/).

References

Afgan, E., Sloggett, C., Goonasekera, N., Makunin, I., Benson, D., Crowe, M., Gladman, S., Kowsar, Y., Pheasant, M. and Horst, R. (2015). Genomics virtual laboratory: a practical bioinformatics workbench for the cloud. *Plos One* **10**, e0140829.

Baddeley, A. and Turner, R. (2005). spatstat: An R package for analyzing spatial point patterns. *J Stat Softw* **12**, 1-42.

Baddeley, R., Osorio, D. and Jones, C. D. (2001). Colour generalisation by domestic chicks. *Behav Brain Sci* **24**, 654-654.

Baden, T. (2021). Circuit mechanisms for colour vision in zebrafish. *Curr Biol* **31**, R807-R820.

Baden, T. and Osorio, D. (2019). The retinal basis of vertebrate color vision. *Annu Rev Vis Sci* **5**, 177-200.

Barthel, L. K. and Raymond, P. A. (2000). In situ hybridization studies of retinal neurons. *Methods Enzymol* **316**, 579-90.

Bates, D., Machler, M., Bolker, B. M. and Walker, S. C. (2015). Fitting Linear Mixed-Effects Models using lme4. *J Stat Softw* **67**, 1-48.

Bolger, A. M., Lohse, M. and Usadel, B. (2014). Trimmomatic: a flexible trimmer for Illumina sequence data. *Bioinformatics* **30**, 2114-2120.

Brokovich, E., Ben-Ari, T., Kark, S., Kiflawi, M., Dishon, G., Iluz, D. and Shashar, N. (2010). Functional changes of the visual system of the damselfish *Dascyllus marginatus* along its bathymetric range. *Physiol Behav* **101**, 413-421.

Carleton, K. L., Escobar-Camacho, D., Stieb, S. M., Cortesi, F. and Marshall, N. J. (2020). Seeing the rainbow: mechanisms underlying spectral sensitivity in teleost fishes. *J Exp Biol* **223 (8)**, jeb193334.

Castiglione, G. M. and Chang, B. S. W. (2018). Functional trade-offs and environmental variation shaped ancient trajectories in the evolution of dim-light vision. *Elife* **7**, e35957.

Caves, E. M., Green, P. A., Zipple, M. N., Peters, S., Johnsen, S. and Nowicki, S. (2018). Categorical perception of colour signals in a songbird. *Nature* **560**, 365-367.

Champ, C., Wallis, G., Vorobyev, M., Siebeck, U. and Marshall, J. (2014). Visual acuity in a species of coral reef fish: *Rhinecanthus aculeatus*. *Brain Behav Evolut* **83**, 31-42.

Champ, C. M., Vorobyev, M. and Marshall, N. J. (2016). Colour thresholds in a coral reef fish. *Roy Soc Open Sci* **3**, 160399.

Chan, T., Lee, M. and Sakmar, T. P. (1992). Introduction of hydroxyl-bearing amino acids causes bathochromic spectral shifts in rhodopsin. Amino acid substitutions responsible for red-green color pigment spectral tuning. *J Biol Chem* **267**, 9478-80.

Cheney, K. L., Green, N. F., Vibert, A. P., Vorobyev, M., Marshall, N. J., Osorio, D. C. and Endler, J. A. (2019). An Ishihara-style test of animal colour vision. *J Exp Biol* **222**, jeb189787.

Cheney, K. L., Newport, C., McClure, E. C. and Marshall, N. J. (2013). Colour vision and response bias in a coral reef fish. *J Exp Biol* **216**, 2967-2973.

Chinen, A., Matsumoto, Y. and Kawamura, S. (2005). Reconstitution of ancestral green visual pigments of zebrafish and molecular mechanism of their spectral differentiation. *Mol Biol Evol* **22**, 1001-10.

Coimbra, J. P., Marceliano, M. L., Andrade-da-Costa, B. L. and Yamada, E. S. (2006). The retina of tyrant flycatchers: topographic organization of neuronal density and size in the ganglion cell layer of the great kiskadee *Pitangus sulphuratus* and the rusty margined flycatcher *Myiozetetes cayanensis* (Aves: Tyrannidae). *Brain Behav Evol* **68**, 15-25.

Coimbra, J. P., Nolan, P. M., Collin, S. P. and Hart, N. S. (2012). Retinal ganglion cell topography and spatial resolving power in penguins. *Brain Behav Evol* **80**, 254-68.

Coimbra, J. P., Trevia, N., Marceliano, M. L., da Silveira Andrade-Da-Costa, B. L., Picanco-Diniz, C. W. and Yamada, E. S. (2009). Number and distribution of neurons in the retinal ganglion cell layer in relation to foraging behaviors of tyrant flycatchers. *J Comp Neurol* **514**, 66-73.

Collin, S. P. and Collin, H. B. (1988). Topographic analysis of the retinal ganglion cell layer and optic nerve in the sandlance *Limnichthyes fasciatus* (Creeiidae, Perciformes). *J Comp Neurol* **278**, 226-41.

Collin, S. P., Knight, M. A., Davies, W. L., Potter, I. C., Hunt, D. M. and Trezise, A. E. (2003). Ancient colour vision: multiple opsin genes in the ancestral vertebrates. *Curr Biol* **13**, R864-5.

Collin, S. P. and Pettigrew, J. D. (1988). Retinal ganglion cell topography in teleosts: a comparison between nissl-stained material and retrograde labelling from the optic nerve. *J Comp Neurol* **276**, 412-422.

Collin, S. P. and Pettigrew, J. D. (1989). Quantitative comparison of the limits on visual spatial resolution set by the ganglion cell layer in twelve species of reef teleosts. *Brain Behav Evolut* **34**, 184-92.

Cortesi, F., Mitchell, L. J., Tettamanti, V., Fogg, L. G., de Busserolles, F., Cheney, K. L. and Marshall, N. J. (2020). Visual system diversity in coral reef fishes. *Semin Cell Dev Biol* **106**, 31-42.

Dalton, B. E., Loew, E. R., Cronin, T. W. and Carleton, K. L. (2014). Spectral tuning by opsin coexpression in retinal regions that view different parts of the visual field. *P Roy Soc B-Biol Sci* **281**, 20141980.

Dalton, B. E., Lu, J., Leips, J., Cronin, T. W. and Carleton, K. L. (2015). Variable light environments induce plastic spectral tuning by regional opsin coexpression in the African cichlid fish, *Metriaclima zebra*. *Mol Ecol* **24**, 4193-204.

de Busserolles, F., Cortesi, F., Helvik, J. V., Davies, W. I. L., Templin, R. M., Sullivan, R. K. P., Michell, C. T., Mountford, J. K., Collin, S. P., Irigoien, X. et al. (2017). Pushing the limits of photoreception in twilight conditions: The rod-like cone retina of the deep-sea pearlsides. *Sci Adv* **3**, eaao4709.

de Busserolles, F., Marshall, N. J. and Collin, S. P. (2014a). The eyes of lanternfishes (Myctophidae, Teleostei): novel ocular specializations for vision in dim light. *J Comp Neurol* **522**, 1618-40.

de Busserolles, F., Marshall, N. J. and Collin, S. P. (2014b). Retinal ganglion cell distribution and spatial resolving power in deep-sea lanternfishes (Myctophidae). *Brain Behav Evol* **84**, 262-76.

de Ibarra, N. H., Giurfa, M. and Vorobyev, M. (2002). Discrimination of coloured patterns by honeybees through chromatic and achromatic cues. *J Comp Physiol A* **188**, 503-512.

Dungan, S. Z., Kosyakov, A. and Chang, B. S. W. (2016). Spectral tuning of killer whale (*Orcinus orca*) rhodopsin: Evidence for positive selection and functional adaptation in a cetacean visual pigment. *Mol Biol Evol* **33**, 323-336.

Escobar-Camacho, D., Taylor, M. A., Cheney, K. L., Green, N. F., Marshall, N. J. and Carleton, K. L. (2019). Color discrimination thresholds in a cichlid fish: *Metriaclima benetos*. *J Exp Biol* **222**, jeb201160.

Fasick, J. I. and Robinson, P. R. (1998). Mechanism of spectral tuning in the dolphin visual pigments. *Biochemistry* **37**, 433-438.

Garza-Gisholt, E., Hemmi, J. M., Hart, N. S. and Collin, S. P. (2014). A comparison of spatial analysis methods for the construction of topographic maps of retinal cell density. *Plos One* **9**, e93485.

Giurfa, M., Vorobyev, M., Brandt, R., Posner, B. and Menzel, R. (1997). Discrimination of coloured stimuli by honeybees: Alternative use of achromatic and chromatic signals. *J Comp Physiol A* **180**, 235-243.

Glaser, E. M. and Wilson, P. D. (1998). The coefficient of error of optical fractionator population size estimates: a computer simulation comparing three estimators. *J Microsc-Oxford* **192**, 163-171.

Haas, B. J., Papanicolaou, A., Yassour, M., Grabherr, M., Blood, P. D., Bowden, J., Couger, M. B., Eccles, D., Li, B. and Lieber, M. (2013). De novo transcript sequence reconstruction from RNA-seq using the Trinity platform for reference generation and analysis. *Nature protocols* **8**, 1494.

Hart, N. S., Partridge, J. C., Cuthill, I. C. and Bennett, A. T. D. (2000). Visual pigments, oil droplets, ocular media and cone photoreceptor distribution in two species of passerine bird: the blue tit (*Parus caeruleus* L.) and the blackbird (*Turdus merula* L.). *J Comp Physiol A Neuroethol Sens Neural Behav Physiol* **186**, 375-387.

Hu, T. J., Wang, G. M., Shen, L. C. and Li, F. (2006). Bionic inspirations of fish-like robots from *Rhinecanthus aculeatus*. *Ieee Icma 2006: Proceeding of the 2006 Ieee International Conference on Mechatronics and Automation, Vols 1-3, Proceedings*, 639-+.

Hughes, A. (1975). A quantitative analysis of the cat retinal ganglion cell topography. *J Comp Neurol* **163**, 107-28.

Hughes, A. (1977). The topography of vision in mammals. In *The Visusl System in Vertebrates; Handbook of Sensory Physiology*, vol. 7/5 (ed. F. Crescitelli), pp. 613-756. Berlin: Springer.

Jones, C. D., Osorio, D. and Baddeley, R. J. (2001). Colour categorization by domestic chicks. *P Roy Soc B-Biol Sci* **268**, 2077-2084.

Karlsson, C., Williis, J. K., Patel, M. and Perera, B. d. (2019). Teleost fish can accurately estimate distance travelled. *bioRxiv*. https://doi.org/10.1101/834341

Katoh, K. and Standley, D. M. (2013). MAFFT multiple sequence alignment software version 7: improvements in performance and usability. *Mol Biol Evol* **30**, 772-780.

Kelber, A., Vorobyev, M. and Osorio, D. (2003). Animal colour vision - behavioural tests and physiological concepts. *Biol Rev* **78**, 81-118.

Kuznetsova, A., Brockhoff, P. B. and Christensen, R. H. B. (2017). lmerTest Package: tests in linear mixed effects models. *J Stat Softw* **82**, 1-26.

Linares, D. and Lopez-Moliner, J. (2016). quickpsy: An R package to fit psychometric functions for multiple groups. *R Journal* **8**, 122-131.

Lind, O. and Kelber, A. (2011). The spatial tuning of achromatic and chromatic vision in budgerigars. *J Vis* **11**, 2.

Luehrmann, M., Stieb, S. M., Carleton, K. L., Pietzker, A., Cheney, K. L. and Marshall, N. J. (2018). Short-term colour vision plasticity on the reef: changes in opsin expression under varying light conditions differ between ecologically distinct fish species. *J Exp Biol* **221** (22): jeb175281.

Matchette, S. R., Cuthill, I. C., Cheney, K. L., Marshall, N. J. and Scott-Samuel, N. E. (2020). Underwater caustics disrupt prey detection by a reef fish. *P Roy Soc B-Biol Sci* **287**, 20192453.

Matsumoto, Y., Fukamachi, S., Mitani, H. and Kawamura, S. (2006). Functional characterization of visual opsin repertoire in Medaka (*Oryzias latipes*). *Gene* **371**, 268-278.

Matthiessen, L. (1882). Ueber die beziehungen, welche zwischen dem brechungsindex des kerncentrums der krystalllinse und den dimensionen des auges bestehen. *Pflugers Arch.* **27**, 510-523.

Mitchell, L., Cheney, K. L., Cortesi, F., Marshall, N. J. and Vorobyev, M. (2017). Triggerfish uses chromaticity and lightness for object segregation. *Roy Soc Open Sci* **4**.

Mullen, K. T. (1985). The contrast sensitivity of human color vision to red green and blue yellow chromatic gratings. *J Physiol-London* **359**, 381-400.

Musilova, Z. and Cortesi, F. (2021). Multiple ancestral and a plethora of recent gene duplications during the evolution of the green sensitive opsin genes (RH2) in teleost fishes. *bioRxiv*. https://doi.org/10.1101/2021.05.11.443711

Musilova, Z., Cortesi, F., Matschiner, M., Davies, W. I. L., Patel, J. S., Stieb, S. M., de Busserolles, F., Malmstrom, M., Torresen, O. K., Brown, C. J. et al. (2019). Vision using multiple distinct rod opsins in deep-sea fishes. *Science* **364**, 588-592.

Musilova, Z., Salzburger, W. and Cortesi, F. (2021). The visual opsin gene repertoires of teleost fishes: evolution, ecology, and function. *Annual Review of Cell and Developmental Biology* **37**, 21.1-21.28.

Nandamuri, S. P., Yourick, M. R. and Carleton, K. L. (2017). Adult plasticity in African cichlids: rapid changes in opsin expression in response to environmental light differences. *Mol Ecol* **26**, 6036-6052.

Neumeyer, C. (1985). An ultraviolet receptor as a 4th receptor type in goldfish color vision. *Naturwissenschaften* **72**, 162-163.

Neumeyer, C. (1986). Wavelength discrimination in the goldfish. *J Comp Physiol A* **158**, 203-213.

Neumeyer, C. (1992). Tetrachromatic color vision in Goldfish - Evidence from color mixture experiments. *J Comp Physiol A* **171**, 639-649.

Olsson, P., Wilby, D. and Kelber, A. (2016). Quantitative studies of animal colour constancy: using the chicken as model. *P Roy Soc B-Biol Sci* **283**: 20160411.

Palczewski, K., Kumasaka, T., Hori, T., Behnke, C. A., Motoshima, H., Fox, B. A., Trong, I. L., Teller, D. C., Okada, T., Stenkamp, R. E. et al. (2000). Crystal structure of rhodopsin: A G protein-coupled receptor. *Science* **289**, 739-745.

Pankhurst, P. M., Pankhurst, N. W. and Montgomery, J. C. (1993). Comparison of behavioral and morphological measures of visual acuity during ontogeny in a teleost fish, *Forsterygion varium*, Tripterygiidae (Forster, 1801). *Brain Behav Evolut* **42**, 178-188.

Parker, A. N., Fritsches, K. A., Newport, C., Wallis, G. and Siebeck, U. E. (2017). Comparison of functional and anatomical estimations of visual acuity in two species of coral reef fish. *J Exp Biol* **220**, 2387-2396.

Parmentier, E., Raick, X., Lecchini, D., Boyle, K., Van Wassenbergh, S., Bertucci, F. and Kever, L. (2017). Unusual sound production mechanism in the triggerfish *Rhinecanthus aculeatus* (Balistidae). *J Exp Biol* **220**, 186-193.

Pignatelli, V., Champ, C., Marshall, J. and Vorobyev, M. (2010). Double cones are used for colour discrimination in the reef fish, *Rhinecanthus aculeatus*. *Biol Letters* **6**, 537-539.

Randall, J. E., Allen, G. R. and Steene, R. C. (1997). Fishes of the Great Barrier Reef and Coral Sea: University of Hawaii Press.

Risner, M. L., Lemerise, E., Vukmanic, E. V. and Moore, A. (2006). Behavioral spectral sensitivity of the zebrafish (Danio rerio). *Vision Res* **46**, 2625-2635.

Ronquist, F., Teslenko, M., van der Mark, P., Ayres, D. L., Darling, A., Höhna, S., Larget, B., Liu, L., Suchard, M. A. and Huelsenbeck, J. P. (2012). MrBayes 3.2: efficient Bayesian phylogenetic inference and model choice across a large model space. *Systematic Biology* **61**, 539-542.

Shand, J. (1997). Ontogenetic changes in retinal structure and visual acuity: a comparative study of coral-reef teleosts with differing post-settlement lifestyles. *Env. Biol. Fish.* **49**, 307-322.

Shi, Y. S., Radlwimmer, F. B. and Yokoyama, S. (2001). Molecular genetics and the evolution of ultraviolet vision in vertebrates. *P Natl Acad Sci USA* **98**, 11731-11736.

Sibeaux, A., Cole, G. L. and Endler, J. A. (2019). Success of the receptor noise model in predicting colour discrimination in guppies depends upon the colours tested. *Vision Res* **159**, 86-95.

Siebeck, U. E., Wallis, G. M. and Litherland, L. (2008). Colour vision in coral reef fish. *J Exp Biol* **211**, 354-60.

Silvasti, S. A., Valkonen, J. K. and Nokelainen, O. (2021). Behavioural thresholds of blue tit colour vision and the effect of background chromatic complexity. *Vision Res* **182**, 46-57.

Simpson, E. E., Marshall, N. J. and Cheney, K. L. (2016). Coral reef fish perceive lightness illusions. *Sci Rep-Uk* **6**, 35335.

Spady, T. C., Parry, J. W., Robinson, P. R., Hunt, D. M., Bowmaker, J. K. and Carleton, K. L. (2006). Evolution of the cichlid visual palette through ontogenetic subfunctionalization of the opsin gene arrays. *Mol Biol Evol* **23**, 1538-47.

Srinivasan, M. V. and Lehrer, M. (1988). Spatial acuity of honeybee vision and its spectral properties. *J Comp Physiol A* **162**, 159-172.

Stieb, S. M., de Busserolles, F., Carleton, K. L., Cortesi, F., Chung, W.-S., Dalton, B. E., Hammond, L. A. and Marshall, N. J. (2019). A detailed investigation of the visual system and visual ecology of the Barrier Reef anemonefish, *Amphiprion akindynos*. *Sci Rep-Uk* **9**, 16459.

Stoddard, M. C., Eyster, H. N., Hogan, B. G., Morris, D. H., Soucy, E. R. and Inouye, D. W. (2020). Wild hummingbirds discriminate nonspectral colors. *P Natl Acad Sci USA* 117 (26) 15112-15122; doi:10.1073/pnas.1919377117

Stone, J., Rapaport, D. H., Williams, R. W. and Chalupa, L. (1981). Uniformity of cell distribution in the ganglion cell layer of prenatal cat retina: implications for mechanisms of retinal development. *Brain Res* **254**, 231-42.

Takahashi, Y. and Ebrey, T. G. (2003). Molecular basis of spectral tuning in the newt short wavelength sensitive visual pigment. *Biochemistry* **42**, 6025-34.

Takenaka, N. and Yokoyama, S. (2007). Mechanisms of spectral tuning in the RH2 pigments of Tokay gecko and American chameleon. *Gene* **399**, 26-32.

Team, R development (2020). RStudio: Integrated Development Environment for R. RStudio, PBC, Boston, MA URL.

Temple, S. E., Manietta, D. and Collin, S. P. (2013). A comparison of behavioural (Landolt C) and anatomical estimates of visual acuity in archerfish (*Toxotes chatareus*). *Vision Res* **83**, 1-8.

Tettamanti, V., de Busserolles, F., Lecchini, D., Marshall, N. J. and Cortesi, F. (2019). Visual system development of the spotted unicornfish, *Naso brevirostris* (Acanthuridae). *J Exp Biol* **222**.

Torres-Dowdall, J., Pierotti, M. E. R., Harer, A., Karagic, N., Woltering, J. M., Henning, F., Elmer, K. R. and Meyer, A. (2017). Rapid and parallel adaptive evolution of the visual system of neotropical midas cichlid fishes. *Mol Biol Evol* **34**, 2469-2485.

Ullmann, J. F., Moore, B. A., Temple, S. E., Fernandez-Juricic, E. and Collin, S. P. (2012). The retinal wholemount technique: a window to understanding the brain and behaviour. *Brain Behav Evol* **79**, 26-44.

van den Berg, C. P., Hollenkamp, M., Mitchell, L. J., Watson, E. J., Green, N. F., Marshall, N. J. and Cheney, K. L. (2020). More than noise: context-dependent luminance contrast discrimination in a coral reef fish (*Rhinecanthus aculeatus*). *J Exp Biol* **223**.

von Frisch, K. (1914). Der Farbensinn und Formensinn der Biene. *Zool Jb (Physiol)* **37**, 1-238.

Vorobyev, M. and Osorio, D. (1998). Receptor noise as a determinant of colour thresholds. *P Roy Soc B-Biol Sci* **265**, 351-358.

West, R. A. (1991). Optical properties of aggregate particles whose outer diameter Is comparable to the wavelength. *Appl Optics* **30**, 5316-5324.

Yokoyama, S. (2000). Molecular evolution of vertebrate visual pigments. *Prog Retin Eye Res* **19**, 385-419.

Yokoyama, S. (2008). Evolution of dim-light and color vision pigments. *Annu. Rev. Genomics Hum. Genet.* **9**, 259-282.

Yokoyama, S. and Jia, H. (2020). Origin and adaptation of green-sensitive (RH2) pigments in vertebrates. *FEBS Open Bio* **10**, 873-882.

Yokoyama, S. and Radlwimmer, B. (1998). The "five-sites" rule and the evolution of red and green color vision in mammals. *Mol Biol Evol* **15**, 560-567.

Yokoyama, S. and Tada, T. (2003). The spectral tuning in the short wavelength-sensitive type 2 pigments. *Gene* **306**, 91-8.

Yokoyama, S., Takenaka, N. and Blow, N. (2007). A novel spectral tuning in the short wavelength-sensitive (SWS1 and SWS2) pigments of bluefin killifish (*Lucania goodei*). *Gene* **396**, 196-202.

Yourick, M. R., Sandkam, B. A., Gammerdinger, W. J., Escobar- Camacho, D., Nandamuri, S. P., Clark, F. E., Joyce, B., Conte, M. A., Kocher, T. D. and Carleton, K. L. (2019). Diurnal variation in opsin expression and common housekeeping genes necessitates comprehensive normalization methods for quantitative real-time PCR analyses. *Molecular Ecology Resources* **19 (6)**, 1447-1460.

Zhou, M., Bear, J., Roberts, P. A., Janiak, F. K., Semmelhack, J., Yoshimatsu, T. and Baden, T. (2020). Zebrafish retinal ganglion cells asymmetrically encode spectral and temporal information across visual space. *Curr Biol* **30**, 2927-2942 e7.

Figures and Tables

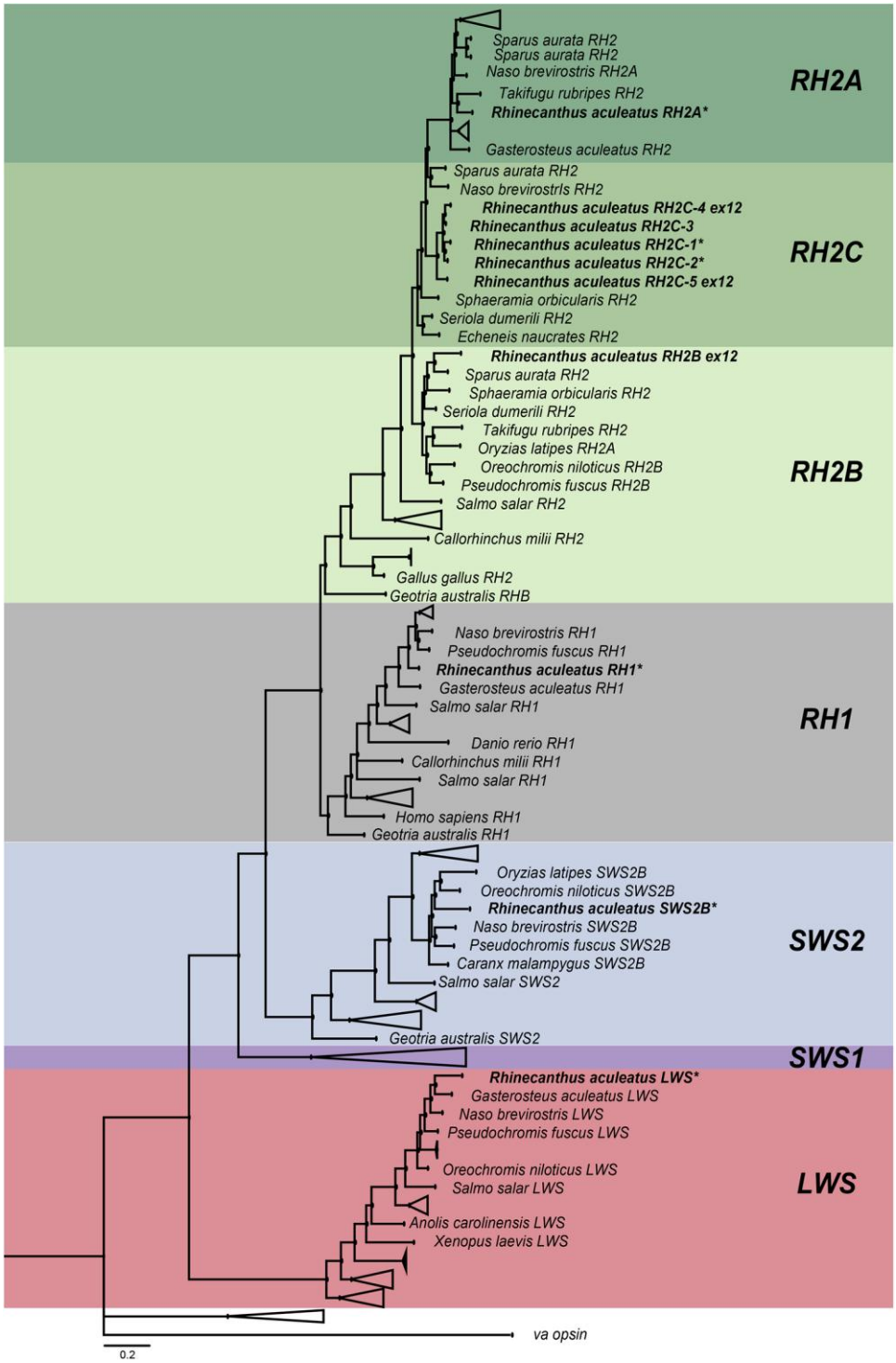

Figure 1: A phylogenetic tree of the visual opsin genes seen in vertebrates. The opsin genes belonging to *Rhinecanthus aculeatus* are highlighted in bold. The sequences extracted from the genome and transcriptome (indicated by *) are positioned within their respective opsin class. *RH1*, rhodopsin 1 (rod opsin); *RH2*, rhodopsin-like 2; *SWS2*, short-wavelength sensitive 2; *LWS*, long-wavelength sensitive; *va*, vertebrate ancient opsin (outgroup). The black circles represent the Bayesian posterior probabilities > 0.8. Scale bar: 0.2 substitutions per site.

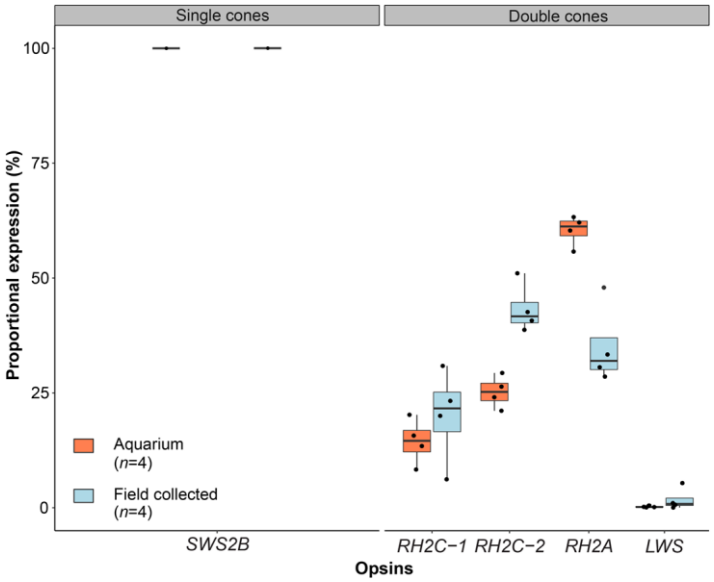

Figure 2: The proportional cone opsin gene expression of *Rhinecanthus aculeatus* individuals collected from the field and the aquarium. All individuals expressed one single cone opsin gene, *SWS2B* and four double cone opsin genes: *RH2C-1, RH2C-2, RH2A*, and *LWS*. The proportional expression of the *RH2* and *LWS* differed between aquarium and field collected individuals.

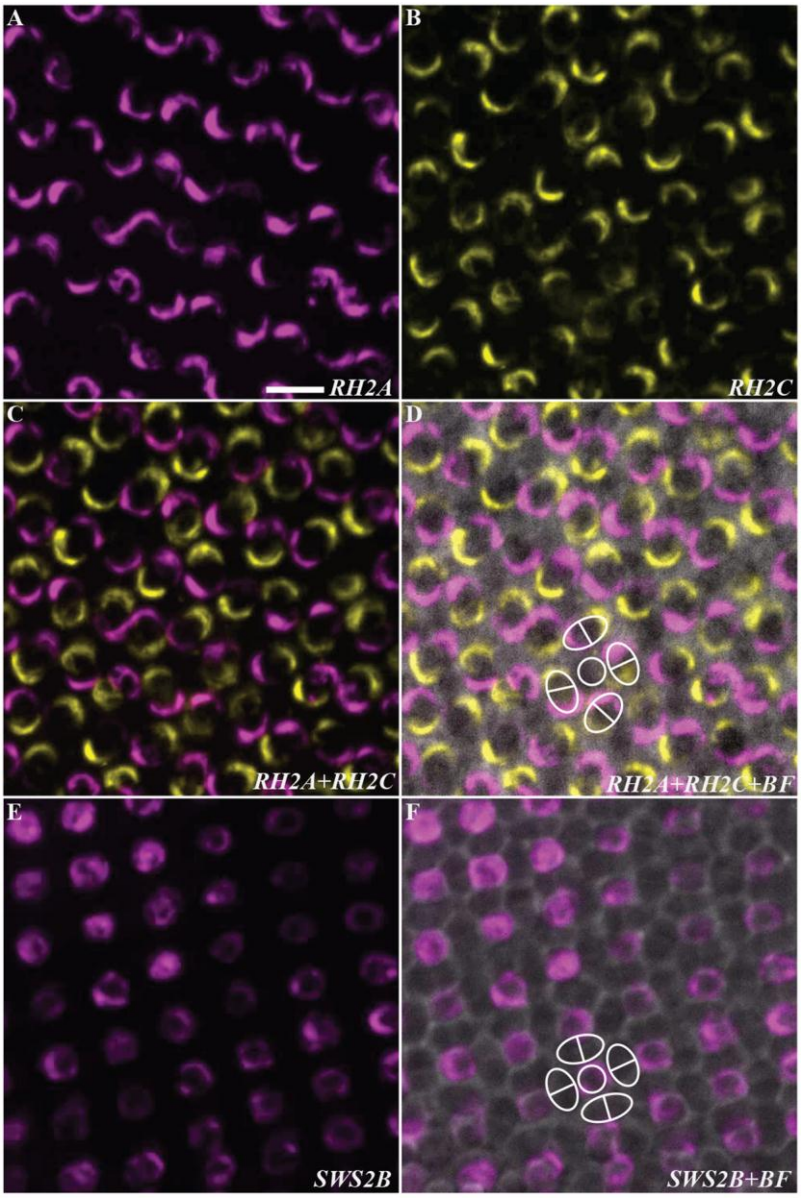

Figure 3: Double-labelling in-situ hybridisation of expressed opsin mRNAs in retinal double cone (A-D) and single cone (E+F) photoreceptors in *Rhinecanthus aculeatus*. (A-D) *RH2A* (magenta) and *RH2C* (yellow) mRNA were expressed in opposite members of double cones across the retina. (E+F) *SWS2B* (magenta) mRNA was exclusively expressed in single cone photoreceptors across the retina. BF: bright field. Scale bar (A-F): 10 µm.

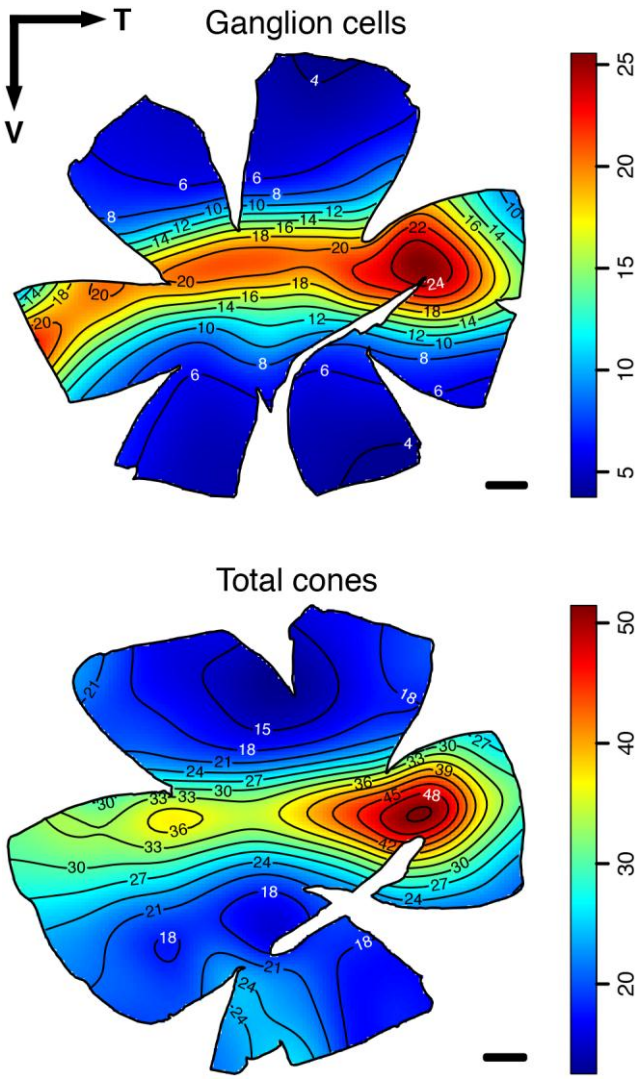

Figure 4: Topographic distribution of ganglion cells and total cone photoreceptors in *Rhinecanthus aculeatus*. The black lines represent iso-density contours and values are expressed in densities x 10^3 cells/mm^2. The black arrow indicates the orientation of the retinas. T = temporal, V = ventral. Scale bars: 1 mm.

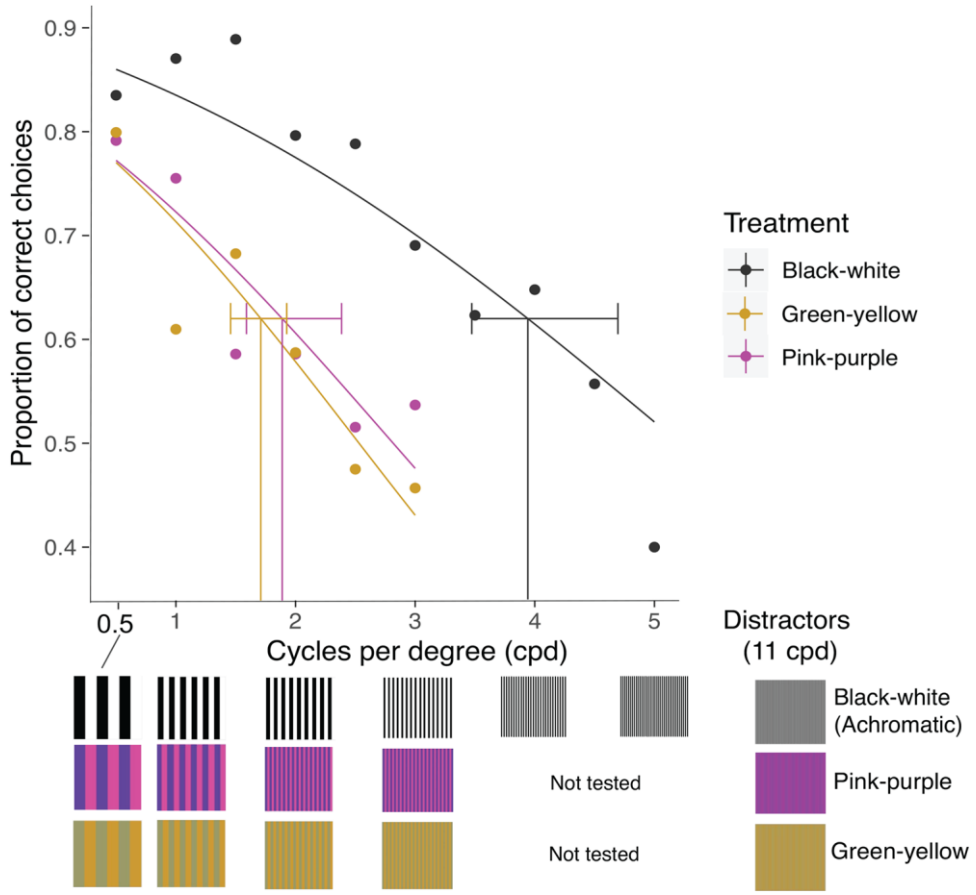

Figure 5: The probability of success in discriminating between target (S+) gratings and distractor gratings. A logistic curve was fitted to pooled data across all fish for each colour combination. Behavioural thresholds (62% correct choice) are shown as vertical lines, error bars are 95% confidence intervals. Data for individual fish are shown in Table S6.

Table 1. Summary of the stereology parameters used for the photoreceptor (PR) and ganglion cells (GC) topography analysis. SL = Standard Length, N = nasal, T = temporal, D = dorsal, V = ventral, Ø = diameter, CE = Schaeffer coefficient of error.

Indiv	SL (cm)	N/T eye Ø (mm)	D/V eye Ø (mm)	Cell counted	Counting frame (µm x µm)	Grid (µm x µm)	CE
1	13.3	9.7	7.8	PR	60 x 60	700 x 700	0.050
2	12.0	9.0	7.0	PR	60 x 60	637 x 637	0.047
3	13.5	8.6	6.3	GC	90 x 90	720 x 720	0.056
3	10.4	8.2	6.3	GC	90 x 90	600 x 600	0.051

Table 2. Summary of the photoreceptor and ganglion cell data using the optical fractionator method**. PR = photoreceptors, DC = double cones, SC = single cones, GC = ganglion cells,** Ø = diameter, SRP = spatial resolving power, cpd = cycles per degree.

Photoreceptors						
Individuals	Total PR	Peak PR (cells/mm^2)	Total DC	Peak DC (cells/mm^2)	Total SC	Peak SC (cells/mm^2)
1	2,034,997	64,167	1,343,688	41,389	691,036	24,722
2	1,851,208	70,278	1,239,849	48,612	610,231	21,667
Ganglion cells						
Individuals	Total GC	Peak GC (cells/mm^2)	Lens Ø (mm)	SRP (cdp)		
3	1,074,112	37,161	3.3	7.2		
4	784,088	40,125	2.8	6.4		

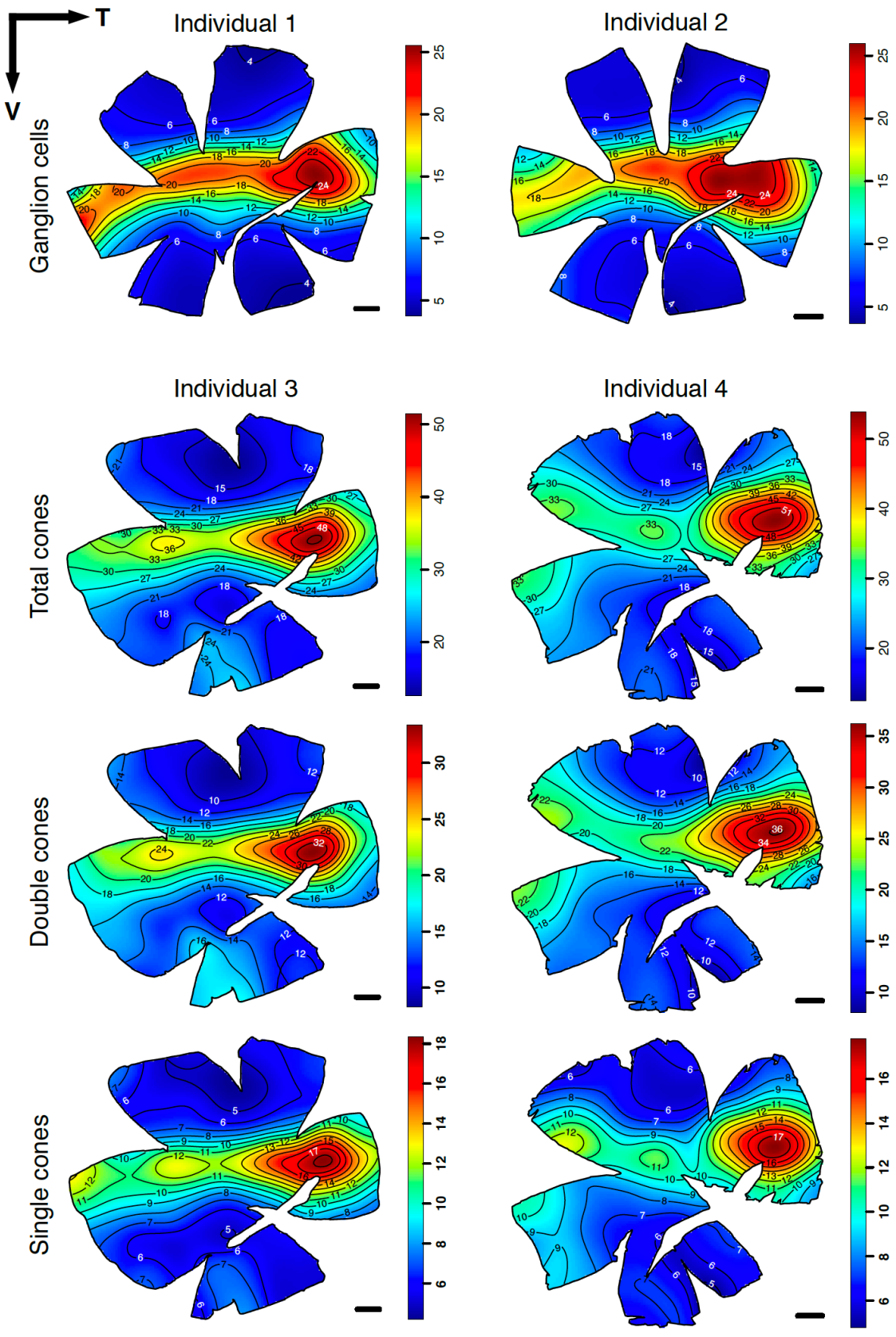

Fig. S1. Intraspecific variability topographic distribution of ganglion cells and cone photoreceptors (single, double and total cones) in *Rhinecanthus aculeatus*. The black lines represent iso-density contours and values are expressed in densities x 10^3 cells/mm^2. The black arrow indicates the orientation of the retinas. T = temporal, V = ventral. Scale bars: 1 mm.

Behavioural measurements of achromatic and chromatic acuity

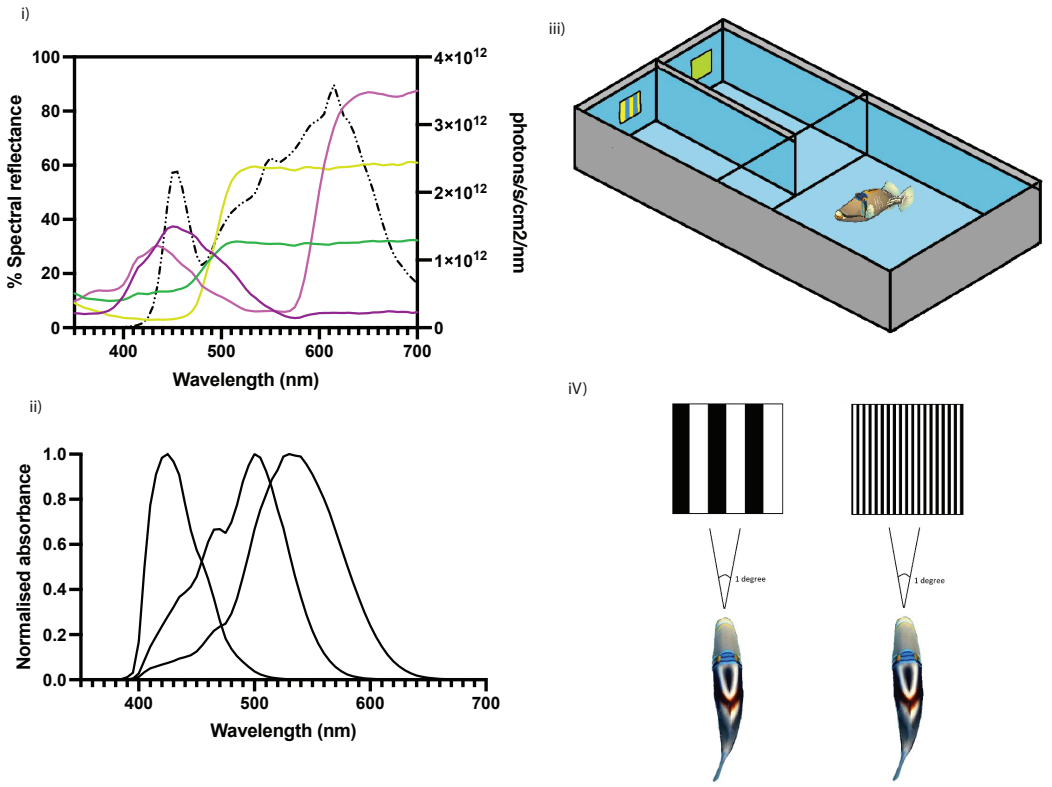

Fig. S2. i) Spectral reflectance of laminated stimuli used in each treatment labelled by color: pink, purple, green and yellow; irradiance of sidewelling lights measured in the testing tanks shown as dashed line; ii) Spectral sensitivities of the three cones in triggerfish, *Rhinecanthus aculeatus*, with a single cone sensitivity of λ_{max} = 413 nm, and double cone sensitivities of λ_{max} = 480 nm and $\lambda = 528_{max}$ nm multiplied by yellow cornea (Cheney et al., 2013); iii) Experimental tank setup; iv) An example of the achromatic (black and white) square-wave gratings: a) 1 cycle per degree; b) 5 cycles per degree.

Table S1. Primers used for probe template synthesis of fluorescence in-situ hybridisation. T7 (forward primer) and T3 (reverse primer) RNA polymerase promoter sequences are shown in bold.

Target gene	Primer	Sequence
RH2A	RH2A_F1 RH2A_R1	5'-**TAATACGACTCACTATAGGG**ATGTACAAGCTCCTGGCTTG-3' 5'-**AATTAACCCTCACTAAAGGG**TCTTTGCAAAGAAGGCGCAC-3'
RH2C-1 & RH2C-2	RH2C_F1 RH2C_R1	5'-**TAATACGACTCACTATAGGG**CCATCAACTTCCTGACGCTA-3' 5'-**AATTAACCCTCACTAAAGGGAGCCAAACACCATCAGGACA**-3'
SWS2B	SWS2B_F1 SWS2B_R1	5'-**TAATACGACTCACTATAGGG**AGAGGCCCCAGATGACTTCT-3' 5'-**AATTAACCCTCACTAAAGGG**ACGGACTGACTCGATGAGGA-3'

Table S2. Summary of transcriptomes, opsin mapping and opsin gene expression of *Rhinecanthus aculeatus.*

			Mapping						**Proportional opsin expression % (normalized to coding sequence length)**						
			Rods	**Single cones (SC)**	**Double cones (DC)**				**Rod vs Cone**		**SC**	**DC**			
Origin	**ID**	**# filtered transcriptome reads**	***RH1* # reads**	***SWS2B* # reads**	***RH2A* # reads**	***RH2C-1* # reads**	***RH2C-1* # reads**	***LWS* # reads**	**R**	**C**	***SWS2B***	***RH2A***	***RH2C-1***	***RH2C-2***	***LWS***
Field	FZ9	10736408	14826	560	1488	1037	1901	44	74.62	25.38	100	33.29	15.65	50.08	0.97
	FZ10	9975040	23638	1390	1876	1894	2376	0	75.77	24.23	100	30.52	26.33	43.15	0.00
	FZ11	6864530	15196	798	654	458	1170	14	83.04	16.96	100	28.49	22.01	48.90	0.60
	1LIT	22709442	136187	18897	26723	3429	22709	3014	79.07	20.93	100	47.86	5.38	41.44	5.32
	Mean	**12571355**	**47696.50**	**5411.25**	**7685.25**	**1704.50**	**8751.67**	**768.00**	**78.13**	**21.87**	**100**	**35.04**	**17.34**	**45.89**	**1.72**
	Se	**3481577.01**	**29879.20**	**4498.64**	**6351.03**	**646.09**	**5229.22**	**748.72**	**1.89**	**1.89**	**-**	**4.39**	**4.55**	**2.12**	**1.22**
Aquarium	LY	21584148	273003	40177	82429	18303	35983	52	60.61	39.39	100	60.27	11.87	27.83	0.04
	SQ	21581834	272743	34687	79679	28871	34329	212	60.47	39.53	100	55.69	6.19	37.97	0.15
	PE	24905208	305271	40809	81017	20063	26989	124	64.30	35.70	100	63.20	14.43	22.28	0.10
	NE	20168834	387049	66207	168363	22443	79481	1170	53.34	46.66	100	62.03	16.11	21.44	0.43
	Mean	**22060006**	**309516.50**	**45470.00**	**102872**	**22420**	**44195.50**	**389.50**	**59.68**	**40.32**	**100**	**60.30**	**17.34**	**45.89**	**0.18**
	S.e.	**1005269.25**	**26948.78**	**7047.68**	**21837.55**	**2311.58**	**11923.10**	**262.22**	**2.29**	**2.29**	**-**	**1.65**	**2.17**	**3.81**	**0.09**

Table S3. Predicted *R. aculeatus* visual pigment peak spectral sensitivities (λ_{max}) compared to reference visual pigments (*O. latipes* RH1; *Oreochromis niloticus,* SWS2B, RH2B, RH2Aalpha, LWS), *R. aculeatus* λ_{max} determined via MSP, and tuning sites and effects considered for predictions. [1] (Matsumoto et al., 2006), [2](Spady et al., 2006), [3](Dungan et al., 2016), [4](Fasick and Robinson, 1998), [5](Yokoyama et al., 2007), [6](Yokoyama and Tada, 2003), [7](Chinen et al., 2005), [8](Yokoyama and Jia, 2020), [9](Cheney et al., 2013)

	RH1	SWS2B	RH2C-1	RH2C-2	RH2A	LWS
Similarity to reference amino acid sequence (%)	94.1	86.1	85.5	85.5	91.5	89.9
Total variable amino acid	21	49	51	51	30	36
Variable amino acid in transmembrane regions	15	32	30	29	18	19
Variable amino acids at known tuning sites	1	5	12	11	8	0
Reference pigment peak absorbance (nm λ_{max})	502[1]	425[2]	472[2]		528[2]	560[2]
Known tuning sites and applied tuning effects (nm)	S299 A (-2)[3,4]	F46V (+8)[5] A109G (-2)[5] G164A (+1)[6] W265T (-29)[5]	M88C (+3)[7] I112V (+1)[7] T266V (-2)[7]	M88C (+3)[7] I112V (+1)[7]	C88A (-3)[7] I112V (+1)[7]	-
Candidate tuning sites – no effects documented	S166 A	C163F S166F S168A	C98A V185C	C98A V185C	A151T	-
Predicted peak absorbance (nm λ_{max})	500	403	474	476	526	560
MSP peak absorbance (nm λ_{max})	498[9]	413[9]	480[9]		528[9]	-

Table S4. Summary of stimuli presented to each fish and in which order, whether the fish was trained to receive a food reward from the Distractor (11 cpd) or the test gratings (0.5-6 cpd), the total number of trials conducted by each fish for each colour (total number of trials = 2438) and calculated discrimination thresholds at 62% correct choice. NA indicates not tested due to time taken to complete treatment 1.

Fish ID	Size (SL, cm)	Treatment 1	S +ve	Threshold (cpd)	Treatment 2	S +ve	Threshold (cpd)
Billy	16	Green-yellow (179)	Control (11 cpd)	2.19	NA	NA	NA
Bitey	10	Pink-purple (120)	Grating	2.45	Green-yellow (167)	Grating	2.17
Diego	16	Achromatic (203)	Grating	4.89	Pink-purple (75)	Grating	2.73
Ernie	17	Achromatic (205)	Control (11 cpd)	5.30	NA	NA	NA
Gilbert	16.5	Green-yellow (184)	Grating	2.71	Achromatic (235)	Grating	5.03
Lyra	10	Pink-purple (120)	Grating	2.95	Green-yellow (167)	Grating	3.04
Mike	15	Green-yellow (188)	Grating	2.58	Pink-purple (167)	Grating	3.27
Sophie	15	Pink-purple (193)	Control (11 cpd)	5.44	Achromatic (235)	Control (11 cpd)	5.44

Further references

Cheney, K. L., Newport, C., McClure, E. C. and Marshall, N. J. (2013). Colour vision and response bias in a coral reef fish. *J Exp Biol* **216**, 2967-2973.

Chinen, A., Matsumoto, Y. and Kawamura, S. (2005). Reconstitution of ancestral green visual pigments of zebrafish and molecular mechanism of their spectral differentiation. *Mol Biol Evol* **22**, 1001-10.

Dungan, S. Z., Kosyakov, A. and Chang, B. S. W. (2016). Spectral tuning of killer whale (orcinus orca) rhodopsin: Evidence for positive selection and functional adaptation in a cetacean visual pigment. *Mol Biol Evol* **33**, 323-336.

Fasick, J. I. and Robinson, P. R. (1998). Mechanism of spectral tuning in the dolphin visual pigments. *Biochemistry* **37**, 433-438.

Matsumoto, Y., Fukamachi, S., Mitani, H. and Kawamura, S. (2006). Functional characterization of visual opsin repertoire in medaka (oryzias latipes). *Gene* **371**, 268-278.

Spady, T. C., Parry, J. W., Robinson, P. R., Hunt, D. M., Bowmaker, J. K. and Carleton, K. L. (2006). Evolution of the cichlid visual palette through ontogenetic subfunctionalization of the opsin gene arrays. *Mol Biol Evol* **23**, 1538-47.

Yokoyama, S. and Jia, H. (2020). Origin and adaptation of green-sensitive (rh2) pigments in vertebrates. *FEBS Open Bio* **10**, 873-882.

Yokoyama, S. and Tada, T. (2003). The spectral tuning in the short wavelength-sensitive type 2 pigments. *Gene* **306**.

Yokoyama, S., Takenaka, N. and Blow, N. (2007). A novel spectral tuning in the short wavelength-sensitive (sws1 and sws2) pigments of bluefin killifish (lucania goodei). *Gene* **396**, 196-202.